Aqueous •OH Oxidation of Highly Substituted Phenols as a Source of Secondary Organic Aerosol

Stephanie Arciva[1], Christopher Niedek[2], Camille Mavis[1], Melanie Yoon[1], Martin Esparza Sanchez[1], Qi Zhang[2], and Cort Anastasio[1*]

[1]Department of Land, Air, and Water Resource, University of California, Davis, CA 95616, United States

[2]Department of Environmental Toxicology, University of California, Davis, CA 95616, United States

**Correspondence to: Cort Anastasio (canastasio@ucdavis.edu)*

Abstract Word Count (150-200 words): 207

Research Article Word Count (limit 7,000 word-equivalent): 5,135 + (300 x 5 figs) = 6,635 words

TOC Art (3.08 in x 1.75 in)

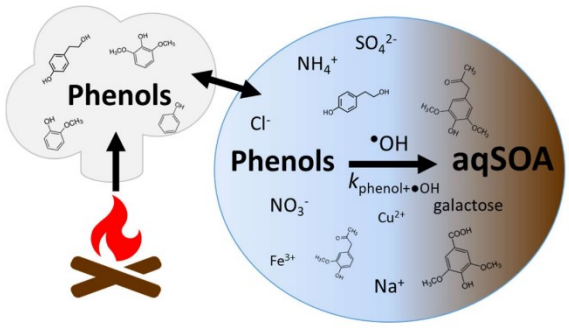

Abstract

Biomass burning (BB) releases large quantities of phenols (ArOH), which can partition into cloud/fog drops and aerosol liquid water (ALW), react, and form aqueous secondary organic aerosol (aqSOA). While simple phenols are too volatile to significantly partition into particle water, highly substituted ArOH partition more strongly and might be important sources of aqSOA in ALW. To investigate this, we measured the •OH oxidation kinetics and aqSOA yields for six highly substituted ArOH from BB. Second-order rate constants are high, in the range (1.9 – 14) × 10^9 M^{-1} s^{-1} at pH 2 and (14 – 20) × 10^9 M^{-1} s^{-1} at pH 5 and 6. Mass yields of aqSOA are also high, with an average (±σ) value of (82 ± 12)%. ALW solutes have a range of impacts on phenol oxidation by •OH: a BB sugar and some inorganic salts suppress oxidation, while a nitrate salt and transition metals enhance oxidation. Finally, we estimated rates of aqueous- and gas-phase formation of SOA from a single highly substituted phenol as a function of liquid water content (LWC), from conditions of cloud/fog (0.1 g-H_2O m^{-3}) to ALW (10 μg-H_2O m^{-3}). Formation of aqSOA is significant across the LWC range, although gas-phase •OH becomes dominant under ALW conditions. We also see a generally large discrepancy between measured and modeled aqueous •OH concentrations across the LWC range.

Keywords

Hydrocarbons, aromatic compounds, oxidation, kinetic parameters, water

Synopsis

Minimal research examines the formation of aqueous secondary organic aerosol (aqSOA) in particle water. This study demonstrates that the $^{\bullet}OH$ oxidation of highly substituted phenols can be an important source of aqSOA in particle water as well as in cloud and fog drops.

Introduction

Atmospheric particulate matter (PM) has important effects on air quality, human health, and climate.[1–4] A portion of these impacts is due to secondary organic aerosol (SOA), which represents a large fraction of particle mass.[5,6] SOA can be formed via the oxidation of volatile organic compounds (VOCs), either in the gas phase or in atmospheric aqueous phases such as cloud/fog drops and aerosol liquid water (ALW).[7–9] One class of VOCs that appears to be important for both gas- and aqueous-phase formation of SOA is phenols (ArOH),[10–12] which are emitted from biomass burning (BB) and formed from the oxidation of aromatic species,[13–16] and react rapidly with several atmospheric oxidants.[17–19]

Hydroxyl radical ($^{\bullet}OH$) is an important atmospheric oxidant in forming SOA,[20–22] although awareness of other oxidants is increasing.[9,23,24] Major sources for $^{\bullet}OH$ in the aqueous phase include the Fenton reaction between Fe(II) and H_2O_2, photolysis of nitrite, nitrate and H_2O_2, mass transport from the gas-phase, and in less acidic conditions, reaction of ozone with superoxide.[9,20,24,25] The major sink for $^{\bullet}OH$ in atmospheric waters is dissolved organic carbon (DOC), with a general rate constant of 3.8×10^8 L mol-C^{-1}.[26] The ratio of sources to sinks determines the steady-state $^{\bullet}OH$ concentration, which controls the rate of formation of aqueous SOA (aqSOA) from hydroxyl radical. Modeled values of [$^{\bullet}OH$] are generally higher than measurements, suggesting models overpredict rates of aqSOA formation from $^{\bullet}OH$-mediated reactions,[26,27] although it is also possible measurements underpredict $^{\bullet}OH$.

Phenols are oxidized in the gas and aqueous phases to form SOA.[18,19,28] In the gas phase, phenol oxidation is primarily by $^{\bullet}OH$ and proceeds through $^{\bullet}OH$ addition, with SOA mass yields between 17 and 86%.[10,17,29] In the aqueous phase, oxidation of ArOH is more complex due to additional oxidants, especially the triplet excited states of organic compounds ($^3C^*$).[12,30] Hydroxyl radical oxidation of ArOH in the aqueous phase also proceeds via $^{\bullet}OH$ addition, with SOA mass yields that range from 59 to 105%, notably higher than for gas-phase reactions,[12,31] probably because of more efficient aqueous formation of oligomers.[17]

Traditionally studied ArOH from BB include phenol (C_6H_5OH), guaiacol (2-methoxyphenol), and syringol (2,6-dimethoxyphenol), which represent the three major phenolic base structures from BB.[13,15,16,25,32] These simple ArOH, however, have moderate Henry's law constants (K_H = $10^3 – 10^4$ M atm^{-1}) and thus are predominantly in the gas phase, even under the relatively high liquid water conditions of clouds and fogs.[33–35] In contrast, highly substituted ArOH, with Henry's law constants of $10^6 – 10^9$ M atm^{-1},[35] partition significantly into the aqueous phase, even under ALW conditions.[36] However, assessing the aqSOA formation potential of highly substituted phenols requires $^{\bullet}$OH rate constants and mass yield data, which have not been reported.

While numerous studies have characterized aqSOA formation under cloud and fog conditions, less is known about aqSOA formation under ALW conditions. Compared to fogs and clouds, where liquid water contents (LWC) are typically on the order of 0.1 g-H_2O m^{-3}, the amount of liquid water on particles is much less abundant (typically 1 – 200 μg m^{-3})[37,38] and contains much higher concentrations of salts, organics, and metal ions.[9,36,38,39] As a result, aqSOA formation in ALW can be different from that in clouds and fogs,[40–43] although this has not been studied for $^{\bullet}$OH-initiated reactions of phenols.

To address these gaps, here we determine second-order rate constants and aqSOA mass yields for six highly substituted ArOH at two pH values (typically pH 2 and 5). We also quantify the impact of different ALW solutes and trace metals on the rate of ArOH oxidation by $^{\bullet}$OH. Finally, we examine how the rate of aqSOA formation from a highly substituted phenol varies over a range of LWC, from cloud/fog to aerosol liquid water conditions.

Methods

Chemicals and Solutions

Hydrogen peroxide (H_2O_2, ≥ 30%), 4-hydroxy-3-methoxyphenylacetone (guaiacylacetone) (96%), vanillyl alcohol (≥ 98%), 2-(4-hydroxyphenyl)ethanol (tyrosol) (98%), syringic acid (≥ 95%), *trans*-ferulic acid (99%), phenol (99%), syringol (99%), guaiacol (≥ 98%), 2-nitrobenzaldehyde (2-NB) (98%), ammonium sulfate (≥ 99%), ammonium nitrate (≥ 99%), sodium chloride (≥ 99%), galactose (≥ 98%), copper(II) sulfate pentahydrate (≥ 98%), and iron(III) chloride (≥ 97%) were purchased from Sigma-Aldrich and used as received. Syringyl

acetone (3,5-dimethoxy-4-hydroxyphenyl)acetone (82%) was synthesized by Carbosynth LLC and used as received. Sulfuric acid (trace metal grade) and acetonitrile (Optima LC-MS grade) were from Fisher Scientific. Chemical solutions were prepared in air-saturated ultrapure Milli-Q water (≥18.2 MΩ cm) from a Millipore Advantage A10 system with an upstream Barnstead activated carbon filter.

Rate constants were determined using a relative rate method (see supplemental Section S1). Solutions were prepared on the day of the experiment (Table S1) and contained 15 μM test compound (i.e., the phenol whose $^{\bullet}OH$ rate constant was being determined), 15 μM reference compound (with a known $^{\bullet}OH$ rate constant), 1.0 mM 2-propanol (2-PrOH), and 10 mM H_2O_2 ($^{\bullet}OH$ precursor). 2-PrOH was added to control the $^{\bullet}OH$ sink and suppress the influence of variable background contaminants on the $^{\bullet}OH$ steady-state concentration; this addition has no effect on the determined rate constant. Prior to rate constant solution preparation, the concentration of hydrogen peroxide in an 18 mM stock solution was determined by absorbance (ε_{240nm}= 38.1 M^{-1} s^{-1})[44] using a Shimadzu UV-Vis spectrophotometer. Solutions were adjusted to pH 2, 5, or 6 using sulfuric acid or sodium hydroxide and were measured using an Orion 420A pH meter.

Illumination and Analysis

The relative rate solution was held in a 5-cm, capped, quartz Spectrocell cuvette, continuously stirred at 20˚C, and illuminated using simulated sunlight from a 1000 W Xe arc lamp with down-stream optical filters.[45] Dark control samples were kept in a separate temperature controlled (20 ˚C) dark chamber. Samples were illuminated until approximately 50% of the initial phenol concentration had reacted (i.e., until time $t_{1/2}$).

During an experiment, 200 μL of solution was removed periodically from the illuminated and dark cells to measure the test and reference chemical concentrations using a Shimadzu High-Performance Liquid Chromatography (HPLC) containing a BetaBasic-18 C_{18} column (250 × 3 mm, 5 μm bead) coupled to a photo-diode array detector (PDA) (Table S2).

We also tested the direct photodegradation of the highly substituted ArOH by illuminating 15 μM solutions without the addition of H_2O_2. Three phenols (ferulic acid, syringic acid, and syringyl acetone) undergo significant direct photodecay on the timescale of our experiments

(Section S2 and Ma et al., Section S4[30]). We corrected measured first-order rate constants for loss of these compounds in the presence of $^{\bullet}OH$ by subtracting the first-order direct photodegradation loss. Guaiacylacetone also undergoes direct photodegradation at a very slow rate,[39] but this is insignificant on the time scale of our experiments and did not require correction.

We measured the photon flux on the day of each experiment using 10 μM 2-nitrobenzaldehyde (2-NB) under the same conditions (including illumination cell) as the relative rate solution.[46]

Relative Rate Method

Following work by Smith et al.,[12] we determined second-order rate constants for our highly substituted ArOH with $^{\bullet}OH$ using a relative rate technique. As shown in the top plot of Figure 1, we monitored the first-order loss of both the test and reference compound during an experiment. We then plotted the loss of test compound versus that of the reference compound to determine the ratio of pseudo-first-order rate constants (i.e., k'_{test}/k'_{ref}) from the slope of the resulting line (Fig 1, bottom plot). The unknown second-order rate constant for the test compound ($k_{test+OH}$) was then determined using:

$$k_{\text{test+OH}} = \frac{k'_{\text{test}}}{k'_{\text{ref}}} \times k_{\text{ref+OH}} \qquad (1)$$

where k_{ref+OH} is the second-order rate constant for the reference compound (Table S3). Final rate constants (Table S4) were determined as the average (± 1σ) of three or four individual experiments.

aqSOA Mass Yields

The mass yield of aqSOA is the ratio of the mass of aqSOA formed to the mass of starting phenol reacted at a given reaction time. aqSOA mass yields were determined at pH 5 for solutions containing 50 or 100 μM of test compound and 5 or 10 mM H_2O_2. 1 mL of sample was removed periodically from the solution during illumination, while the corresponding dark control was sampled at the start and end of the reaction period. Solutions were illuminated to approximately three phenol half-lives, i.e., until roughly 12% of the initial phenol concentration remained in solution.

The aqSOA mass was determined using High-Resolution Aerosol Mass Spectrometry (HR-AMS) method described previously.[47,48] Each sample solution was spiked with known quantities

137 of ammonium sulfate as an internal standard, aerosolized with a constant output atomizer (TSI,
138 Model 3076) using argon as the carrier gas, and then dried in a silica diffusion drier prior to
139 sampling in an HR-AMS (Aerodyne Res. Inc.). Prior studies from our lab indicate that
140 evaporation of semi-volatile material during aerosolization and drying does not significantly bias
141 the phenolic aqSOA mass.[47,48] The standard AMS data analysis toolkits (SQUIRREL v1.63H
142 and PIKA v1.23H) were used to process the AMS data. The default relative ionization efficiency
143 for organics (RIE = 1.4) and a collection efficiency of 1 for organics and sulfate were used for
144 AMS data processing. Each sample was analyzed in duplicate and reported mass yields at a
145 given time are the average of both runs.

146 **Solute Effects**

147 To test the impact of additional solutes, we measured on the same day the decay kinetics of
148 guaiacylacetone (GA) with and without the addition of a single solute. Similar to our method
149 described above (but without 2-propanol), we prepared one solution containing 15 μM GA and
150 10 mM H_2O_2, and a second solution containing 15 μM GA, 10 mM H_2O_2, and the solute of
151 interest. Both reaction solutions were adjusted to the same pH, either 2 or 5. Solutions were
152 illuminated and sampled periodically until approximately $t_{1/2}$.

153 **Results and Discussion**

154 **Hydroxyl Radical Kinetics for Highly Substituted Phenols**

155 Our measured rate constants for the reactions of highly substituted ArOH with $^{\bullet}$OH are high and
156 range from (1.9 – 14) × 10^9 M^{-1} s^{-1} at pH 2 (Figure 2). The least substituted phenol, tyrosol,
157 reacts the slowest with $^{\bullet}$OH, while aromatic ring substitution increases the rate of reaction, such
158 that phenols with a guaiacol and syringol base structure are more reactive. A likely reason for
159 this increase in $^{\bullet}$OH reactivity is the electron-donating effects from additional phenol
160 substituents.[49] Smith et al.[12] previously determined second-order rate constants for the aqueous
161 oxidation of six simple ArOH with $^{\bullet}$OH; rate constants at pH 2 ranged from (1.8 – 15) × 10^9 M^{-1}
162 s^{-1}, in the same range as values for our phenols.

163 We also measured rate constants at pH 5 or 6 for highly substituted ArOH. We used pH 5 for
164 most compounds, but pH 6 for syringic acid and ferulic acid so that the carboxylic acid groups
165 would be mostly deprotonated: while the pK_a for a phenoxyl hydrogen is typically near 10,[50] the

166 carboxylic acid groups on ferulic acid and syringic acid have pK_a values of 4.6 and 4.2,
167 respectively.[51] Across all six of the phenols, rate constants at pH 5 and 6 are in the range of (14 –
168 25) × 10^9 M^{-1} s^{-1} and there is no apparent difference between rate constants at pH 5 or 6.

169 In general, rate constants for highly substituted ArOH are higher at pH 5/6 than at pH 2. For
170 tyrosol, the rate constant at pH 5 is 7.4 times higher than at pH 2 (Figure 2). $^{\bullet}$OH rate constants
171 determined by Smith et al.[12] for C_6H_5OH demonstrate a similar pH dependence, where the rate
172 constant at pH 5 is 8.3 times higher than at pH 2. The other highly substituted phenols show
173 much less of a pH dependence, with an average (± 1σ) pH 5 / pH 2 rate constant ratio of 2.0 (±
174 0.2). This trend was also observed for guaiacol and syringol, with ratios of 2.4 and 1.3,
175 respectively.[12] However, because uncertainties are quite large (mostly because of uncertainty in
176 the reference rate constants; Table S3), the rate constants at pH 2 and 5 (or 6) for highly
177 substituted ArOH are not statistically different for a given phenol except for tyrosol. This may be
178 because the rate constants of highly substituted ArOHs with $^{\bullet}$OH approach the diffusion limit.[52]

179 To explore the pH dependence of the $^{\bullet}$OH rate constants, we measured phenol loss kinetics in
180 solutions containing both guaiacylacetone (GA) and guaiacol (GUA) between pH 1 and 5 (Table
181 S5). To account for differences in the photon flux, we divided the pseudo-first order rate
182 constants for loss of GA (k'_{GA}) and GUA (k'_{GUA}) by the photolysis rate constant (j_{2NB}) of our
183 chemical actinometer, 2-nitrobenzaldehyde, which we measured each experiment day. We also
184 divided pseudo-first order rate constants for GA and GUA loss by [H_2O_2], which we sometimes
185 varied. Figure S1 shows these normalized rate constants as a function of pH as well as the ratio
186 k'_{GA}/k'_{GUA}. The rate constant for GA loss changes very little with pH, but that for GUA loss
187 increases with pH. The ratio k'_{GA}/k'_{GUA} follows a sigmoidal curve, with larger ratios at low pH
188 (e.g., approximately 1.5 at pH 2), that decline with increasing pH to approximately 0.8 at pH 3,
189 and remain at this value in less acidic solutions. This difference in the ratio appears driven by the
190 oxidation kinetics of GUA at different pH values, but we do not understand the mechanism for
191 this change in reactivity with acidity.

192 To explore whether phenol rate constants with $^{\bullet}$OH could be predicted from oxidation potentials,
193 we constructed quantitative structure-activity relationships (QSARs) using oxidation potentials
194 (E_{OX}) previously measured using cyclic voltammetry (CV) and modeled using Gaussian software
195 (Section S3).[30] For each QSAR we combined our rate constant data for highly substituted

196 phenols with rate constants for simple phenols by Smith et al.[12] (Table S5). As shown in Figure
197 S2, rate constants with •OH generally increase as E_{OX} decreases (i.e., as phenols are more easily
198 oxidized), but the correlations only range from non-existent (R^2 = 0.06 at pH 5) to moderate (R^2
199 = 0.41 at pH 2) with measured oxidation potentials. Using Gaussian E_{OX} values gives better
200 (though not great) correlations (R^2 = 0.19 and 0.53 at pH 5 and 2, respectively), consistent with
201 the equivalent QSARs based on rate constants for ArOH with triplet excited states.[30]

202 **SOA Mass Yields**

203 We used aerosol mass spectrometry to measure aqueous SOA mass yields for the reactions of
204 highly substituted ArOH with •OH at one, two, and three half-lives (Section S4 and Figure S3).
205 Averaged across each of these time points for each phenol, aqSOA mass yields range from 66 to
206 98% (Figure 3), with an overall ArOH average (± 1σ) value of 82 (± 12)%. The aqSOA mass
207 yield was highest for tyrosol (98%) and lowest for syringic acid (67%), but there is no apparent
208 trend between the extent (or type) of phenol substitution and aqSOA mass yields for our data.
209 This is also true if we consider results across our six highly substituted ArOH as well as for six
210 simpler BB ArOH studied previously with •OH, as shown in Figure S4. Across all 12 of these
211 phenols, the average (± 1σ) aqSOA mass yields is 87 (± 17)%.[12,31]

212 Aqueous reactions of ArOH with •OH produce higher SOA mass yields than phenols reacting
213 with •OH in the gas phase, where yields range from 10 to 50%.[10,11,49] This is probably because
214 fragmentation is more frequent in the gas phase, while aqueous-phase oxidation results in more
215 functionalization and oligomerization.[17]

216 Our aqSOA yields for highly substituted phenols reacting with •OH are similar to values
217 measured for the same six phenols reacting with a triplet excited state ($^3C^*$), where yields ranged
218 from 59 to 99%, and had an average (± 1σ) yield of 83 (± 14)%.[12,30] In addition to having similar
219 averages, the phenolic aqSOA mass yields for the •OH and $^3C^*$ reactions are fairly well
220 correlated, as shown in Figure S5 and S6. This suggests that differences in phenol structure are
221 more important in determining the efficiency of aqSOA formation than are differences in the
222 oxidant.

223 **Solute Effects on Phenol-•OH Kinetics**

224 Unlike the relatively dilute conditions of clouds and fog drops, solute concentrations are much
225 higher in ALW and this might impact phenol-$^{\bullet}$OH kinetics. Major inorganic species common in
226 aerosols include ammonium sulfate ($(NH_4)_2SO_4$), ammonium nitrate (NH_4NO_3), and sodium
227 chloride (NaCl).[36] BB particles also contain large amounts of cellulose-derived sugars, including
228 levoglucosan and galactose (a hydrolyzed isomer of levoglucosan).[16,53] In addition, redox-active
229 trace metals such as Fe and Cu are also common components of atmospheric aerosols that may
230 influence oxidation kinetics.[54,55]

231 To better understand how these different components in ALW might impact oxidation kinetics,
232 we measured the effects of solutes on the $^{\bullet}$OH-mediated loss of guaiacylacetone (GA). To assess
233 this, we measured the pseudo-first-order rate constants for decay of GA in the presence of added
234 solute ($k'_{GA,solute}$) and without solute (k'_{GA}) on the same day. Then, we examined the ratio
235 $k'_{GA,solute}/k'_{GA}$ to determine the solute impact on GA loss by $^{\bullet}$OH: a ratio above one indicates
236 enhanced GA decay, while values below one indicate suppression.

237 As shown in Figure 4, the addition of 0.5 M NH_4NO_3 increases GA loss by factors of 11 and 20
238 at pH 2 and 5, respectively, a result of NO_3^- photolysis forming additional $^{\bullet}$OH,[56] as observed in
239 recent work.[30,57] In contrast, 2.0 M $(NH_4)_2SO_4$ suppresses phenol decay, yielding ratios of 0.4
240 and 0.5 at pH 2 and 5, respectively, likely because of suppression due to the high ionic strength
241 of the GA-$^{\bullet}$OH reaction. The impact of 2.0 M NaCl depends on solution acidity. At pH 2, NaCl
242 enhances phenol decay by a factor of 2, likely due to the formation of chlorine radicals that react
243 with GA.[32] In contrast, at pH 5 NaCl suppresses GA loss, likely because of an ionic strength
244 suppression. A previous study found that increasing ionic strength with sodium perchlorate
245 ($NaClO_4$) caused a small enhancement in the $^{\bullet}$OH-mediated loss of several organics (butanol,
246 propanol, and acetone),[36] but we found no previous studies that examined the ionic strength
247 effect on $^{\bullet}$OH reactions with phenols. The different results between our work and previous work
248 might be due to differences in salt or organic compounds.[36,41]

249 We also measured the impact of galactose ($C_6H_{12}O_6$), a cellulose-derived sugar from biomass
250 burning, on GA degradation. Because $^{\bullet}$OH directly reacts with galactose ($k = 2 \times 10^9$ M^{-1} s^{-1}),[53,58]
251 the addition of 1.0 mM galactose decreases the steady-state concentration of $^{\bullet}$OH and slows GA
252 oxidation kinetics (Figure 4). The measured ratios of $k'_{GA,solute}/k'_{GA}$ with 1.0 mM galactose are
253 0.29 at pH 2 and 0.34 at pH 5 (Figure 4). However, based on the $^{\bullet}$OH rate constants and

concentrations of the organics in our solutions, we calculate that the ratios should be 0.05 and 0.10 at pH 5 and 2, respectively, i.e., roughly 6 and 3 times lower than measured. This discrepancy might be due to organic contaminants in our reaction solutions, which would decrease the impact of galactose, i.e., give a ratio closer to 1. For the calculated ratios to equal the measured ratios would require an organic contaminant concentration of 200 μmol-C L^{-1}, assuming a general $^{\bullet}OH$-organic reaction rate constant of 3.8×10^8 L mol-C^{-1}.[26] However, based on our past work, organic contaminant concentrations in our typical lab blanks range from 20 – 100 μmol-C L^{-1},[59] suggesting that organic contaminants alone cannot explain the discrepancy between the measured and modeled impacts of galactose.

Finally, we examine the impact of two transition metals. As shown in Figure 4, 20 μM iron(III) chloride enhances GA loss at pH 2 and, especially, at pH 5. This is probably a result of Fe(III) direct photoreactions, which form $^{\bullet}OH$ and Fe(II);[60,61] at pH 5, direct photodegradation of $Fe(OH)^{2+}$, and possibly Fe-phenol complexes, are likely significant. Iron can also enhance $^{\bullet}OH$ formation through Fe(III) reduction by $HO_2^{\bullet}/^{\bullet}O_2^{-}$ to make Fe(II), which reacts with the 10 mM H_2O_2 in our solutions to make additional $^{\bullet}OH$ via the Fenton reaction.[62–64] The addition of 10 μM copper(II) sulfate enhances GA loss kinetics at pH 5, but does not significantly impact GA loss kinetics at pH 2 (Figure 4). At pH 5, superoxide ($^{\bullet}O_2^{-}$) rapidly reduces Cu(II) to Cu(I), allowing copper to generate $^{\bullet}OH$ by a Fenton-like reaction with the 10 mM H_2O_2.[62,65] In contrast, at pH 2 the major form of $^{\bullet}O_2^{-}$ is $HO_2^{\bullet}$ (the conjugate acid of $^{\bullet}O_2^{-}$, with a pK_a of 4.8),[66] which reduces Cu(II) more slowly, leading to a lower Cu(I) concentration and a slower Fenton-like rate of $^{\bullet}OH$ formation.[67]

The impacts of these solutes on GA decay in $^{\bullet}OH/H_2O_2$ solutions are sometimes markedly different from their recently reported impacts on GA decay by triplet excited states.[30] As shown in Figure S7, while inorganic salts suppress the $^{\bullet}OH$ oxidation of GA, they do not significantly affect GA oxidation by triplets (except for ammonium nitrate, which enhances reactivity in both cases). Additionally, 0.9 M galactose does not impact triplet kinetics, but significantly decreases the concentration of $^{\bullet}OH$ and resulting GA degradation. Trace metals also generally have different impacts on GA oxidation by $^{\bullet}OH$ and $^3C^*$, though this can also depend on pH. For example, $CuSO_4$ significantly suppresses phenol loss by triplet excited states, a result of Cu(I) reducing the GA phenoxyl radical (produced by the triplet-GA reaction) back to GA.[68,69] In the

case of the •OH-GA reaction, the major initial reaction intermediate is a hydroxycyclohexadienyl radical, which is not reduced back to GA by Cu(I).[70] Thus Cu does not suppress GA loss in •OH/H_2O_2 solutions at pH 2 and enhances GA loss at pH 5, a consequence of •OH formation by Cu(I) and H_2O_2. Our observation that a given solute can have very different impacts on GA decay by •OH or triplet excited states indicates that the effects of solutes in aerosol liquid water depend on oxidation pathway. This complicates predicting reaction kinetics in particle water from results in more dilute solution.

Atmospheric Implications

Laboratory and field studies indicate that aqSOA from phenols can be important in air influenced by biomass burning, in part driven by hydroxyl radical.[10,17,71–73] However, the rate of aqSOA formation by •OH depends on the •OH concentration and there are often large differences between measured and modeled values of [•OH] in atmospheric waters.[26,74] To examine this issue, we start by compiling measured and modeled aqueous •OH concentrations as a function of liquid water content (or, equivalently, the ratio of dry PM mass to liquid water mass). Figure 5 shows that modeled values can be several orders of magnitude larger than measurements and this discrepancy persists across the atmospheric range of liquid water contents. Even within the models, [•OH(aq)] can vary by a factor of 100 at a given LWC. In part, this is because some models assume that aqueous •OH is in Henry's law equilibrium with gas-phase •OH, which erroneously leads to very high •OH(aq) concentrations (Figure S8). Because the lifetime of •OH in drops and particles is very short (μs to ns)[24,26,32,45] compared to the time scale of mass transport from the gas phase (on the order of seconds), aqueous •OH will be present well below its predicted Henry's law concentration. Finally, the green line in Figure 5 is an extrapolation from Kaur et al.[24] based on measured [•OH(aq)] in a series of dilutions of a winter particle sample from Davis; this prior extrapolation fits the marine particle data at very low LWC reasonably well.

We next examine how the discrepancy between measured and modeled [•OH(aq)] affects the formation of aqSOA. To simplify our calculations, we consider only a single phenol, syringol acetone (SA), at a total initial concentration of 5 μg m^{-3} to represent the sum of highly substituted ArOH in regions of significant BB.[75] We assume SA partitions between the gas and

aqueous phases following Henry's law equilibrium (K_H at 278 K = 6.1 x 10^8 M atm^{-1});[35] since the chemical reaction lifetime of SA is much longer than the characteristic time for mass transport, this is a reasonable assumption. We also assume a constant PM mass concentration of 10 μg m^{-3} and allow the LWC to vary from approximately 1 g m^{-3} (a thick cloud or fog) to 10^{-6} g m^{-3} (an aerosol with little liquid water). We allow syringyl acetone to react in the aqueous phase with $^{\bullet}$OH (using measured and modeled $^{\bullet}$OH concentrations from the top panel of Figure 5) as well as in the gas phase, where the $^{\bullet}$OH concentration is constant at 1×10^6 molecules cm^{-3}. The aqSOA mass yield for SA is 86% (Figure 3), while we assume the corresponding value in the gas phase is 32%, based on data from simpler phenols.[17]

The bottom panel of Figure 5 shows the initial rate of SOA formation from the $^{\bullet}$OH oxidation of syringyl acetone as a function of LWC. Mirroring what was seen for hydroxyl radical concentrations, rates of aqSOA calculated using modeled $^{\bullet}$OH(aq) are consistently higher than rates determined with measured $^{\bullet}$OH(aq). In cases where the modeled aqueous $^{\bullet}$OH was determined assuming Henry's law equilibrium, initial rates of aqSOA are ridiculously high, approaching 1000 μg m^{-3}-air hr^{-1}. In contrast, calculated aqSOA rates based on measured $^{\bullet}$OH(aq) are much lower, on the order of 1 μg m^{-3} hr^{-1} under fog/cloud conditions and 0.02-0.3 μg m^{-3} hr^{-1} under ALW conditions. The rate of aqSOA formation decreases only slowly as LWC decreases because the Henry's law constant for SA is high, so this highly substituted phenol remains primarily in the aqueous phase even at low LWCs. We also considered the reaction of gas-phase $^{\bullet}$OH with syringyl acetone as a source of SOA, as shown by the yellow dashed line. The gas-phase reaction of SA does not become important until ALW conditions, when the gas-phase reaction is as important as aqueous oxidation.

Overall, our measurements indicate that the aqueous-phase oxidation of highly substituted ArOH can be a rapid and efficient pathway of SOA formation. Our calculations in Figure 5 show that this processing is especially rapid under cloud and fog conditions but is significant even under the much lower liquid water conditions of aerosols. The results in Figure 5 also reiterate a point made by Arakaki et al.:[26] there is a very large disagreement in measured and modeled aqueous $^{\bullet}$OH concentrations. As the bottom panel of this figure shows, this disagreement leads to very high uncertainties in estimated rates of $^{\bullet}$OH reactions in atmospheric drops and particles.

Resolving this uncertainty will require additional measurements of $^{\bullet}OH$ in ambient samples, especially under ALW conditions, as well as continued model development.

Supporting Information

Individual phenol and $^{\bullet}OH$ kinetic experiments; photodegradation and photoisomerization of phenols; rate constants and oxidation potentials for phenols; data and figures for aqSOA mass yields; comparison of aqSOA mass yields for phenols with $^{\bullet}OH$ and $^{3}C^{*}$; solute effects on phenol oxidation; measured and modeled [$^{\bullet}OH$] in clouds/fog drops and ALW. This information is available free of charge via the Internet at http://pubs.acs.org.

Acknowledgements

This work was funded by the National Science Foundation grant (AGS-1649212), the California Agricultural Experiment Station (Projects CA-D-LAW-6403-RR and CA-D-ETX-2102-H), and by Jastro-Shields Research Awards from UC Davis to S.A. and C.N..

Figures

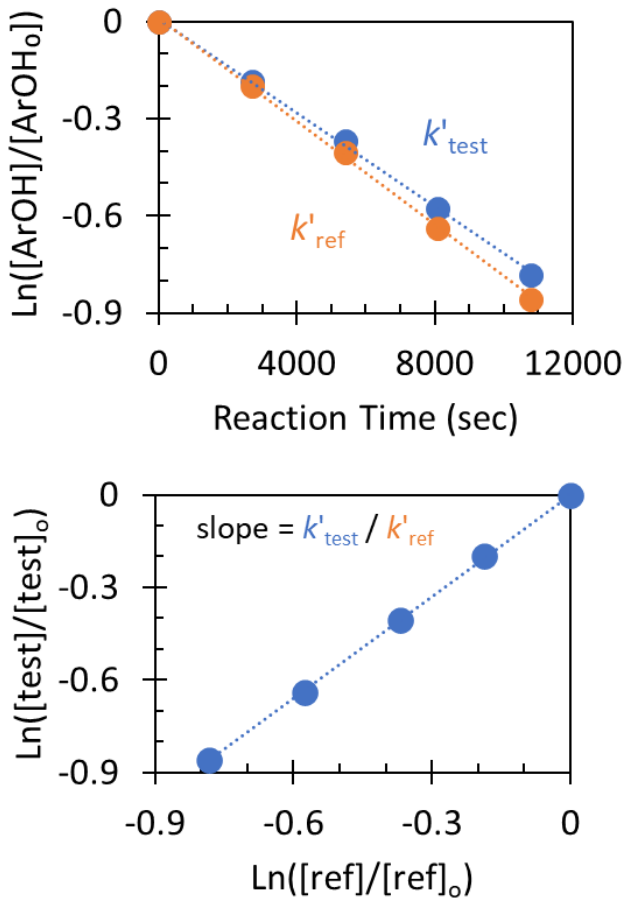

Figure 1. Top panel: Loss of guaiacol (reference phenol; orange circles) and guaiacylacetone (test phenol; blue circles) in the presence of $^{\bullet}$OH under simulated sunlight conditions. There was no loss of either compound in the dark. Bottom panel: Change in concentration of the test compound against the reference compound. The slope is equal to the ratio of the second-order rate constants with hydroxyl radical (Eq. 1).

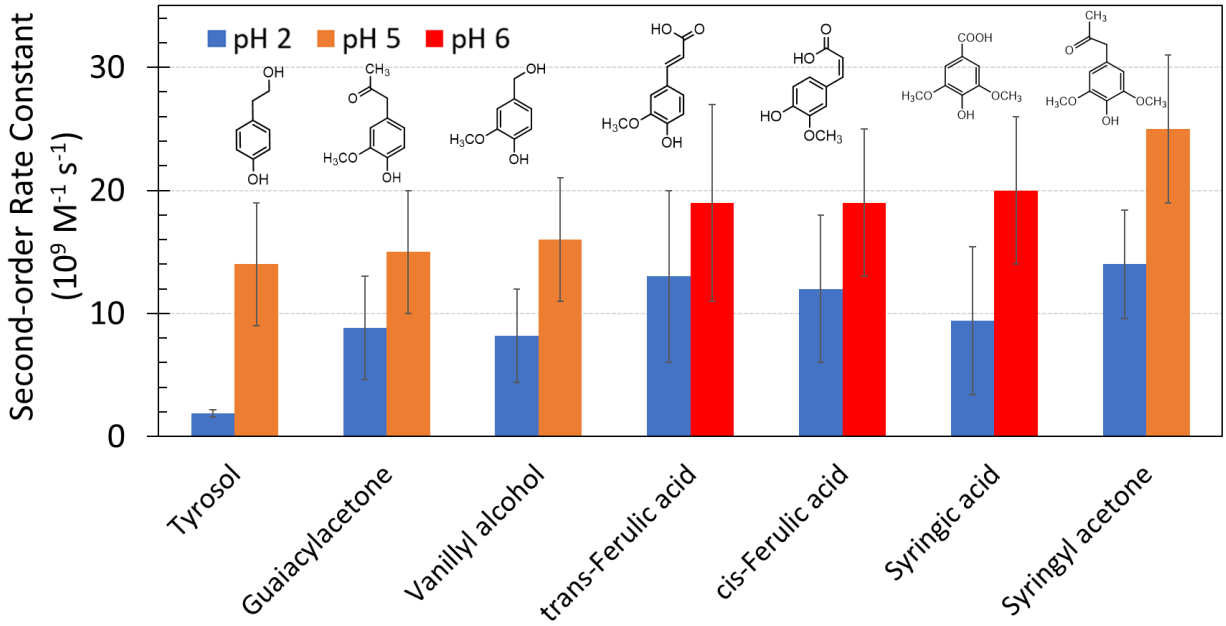

Figure 2. Second-order rate constants for highly substituted ArOH reacting with hydroxyl radical at pH 2 and 5 or 6. Error bars represent ±1 standard error propagated from standard errors in the kinetic plots and in the reference second-order rate constants. Data are listed in Table S4.

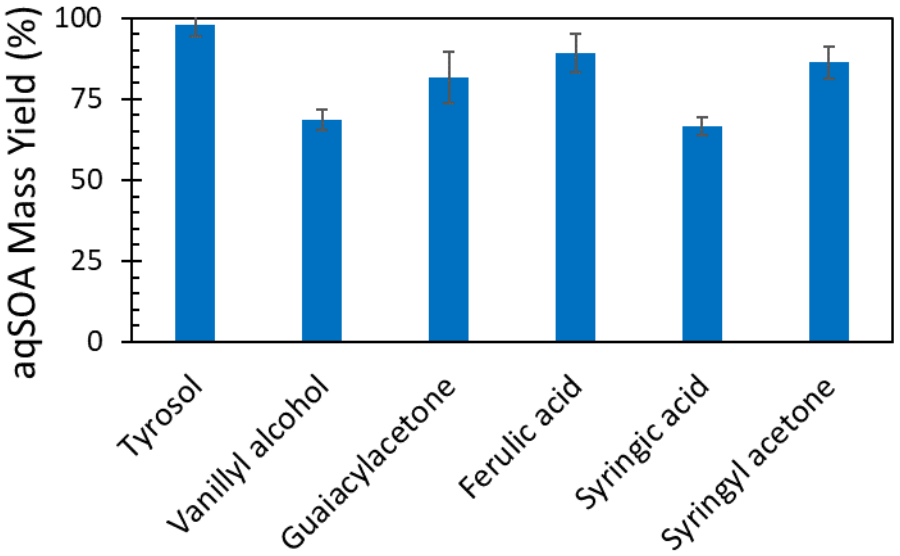

Figure 3. SOA mass yields from the aqueous •OH oxidation of highly substituted ArOH. Error bars represent ±1 standard deviation, calculated from replicate samples at one, two, and three half-lives (i.e., $t_{1/2}$, $2t_{1/2}$, and $3t_{1/2}$).

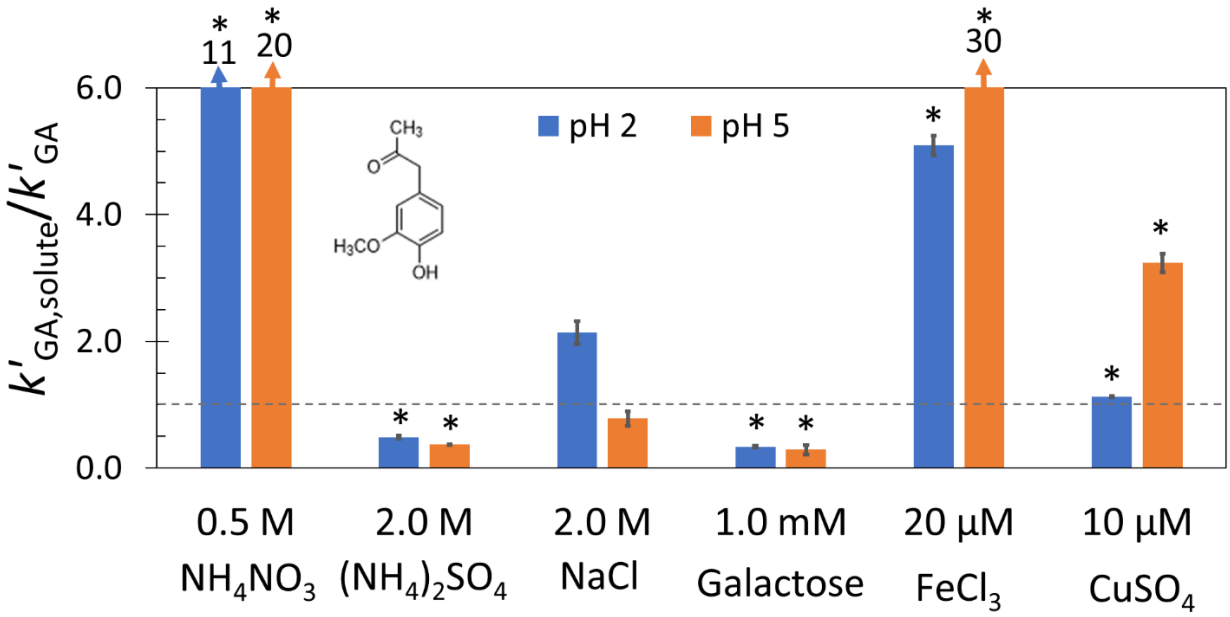

Figure 4. Effect of six solutes on the pseudo-first-order decay of guaiacylacetone (GA) oxidized by •OH at pH 2 (blue bars) and 5 (orange bars). The y-axis ratio represents the pseudo-first order decay of GA in the presence of a given solute ($k'_{GA,solute}$) to the pseudo-first-order decay of GA with no added solute (k'_{GA}), measured on the same day. Error bars represent ±1 standard deviation based on results from duplicate experiments. The grey dotted line represents a ratio of one, i.e., where added solute does not impact GA-•OH kinetics. Bars with an asterisk are statistically different from 1 ($p < 0.05$). The NH_4NO_3 rates have been corrected for internal light screening by nitrate, as described in Section S5.

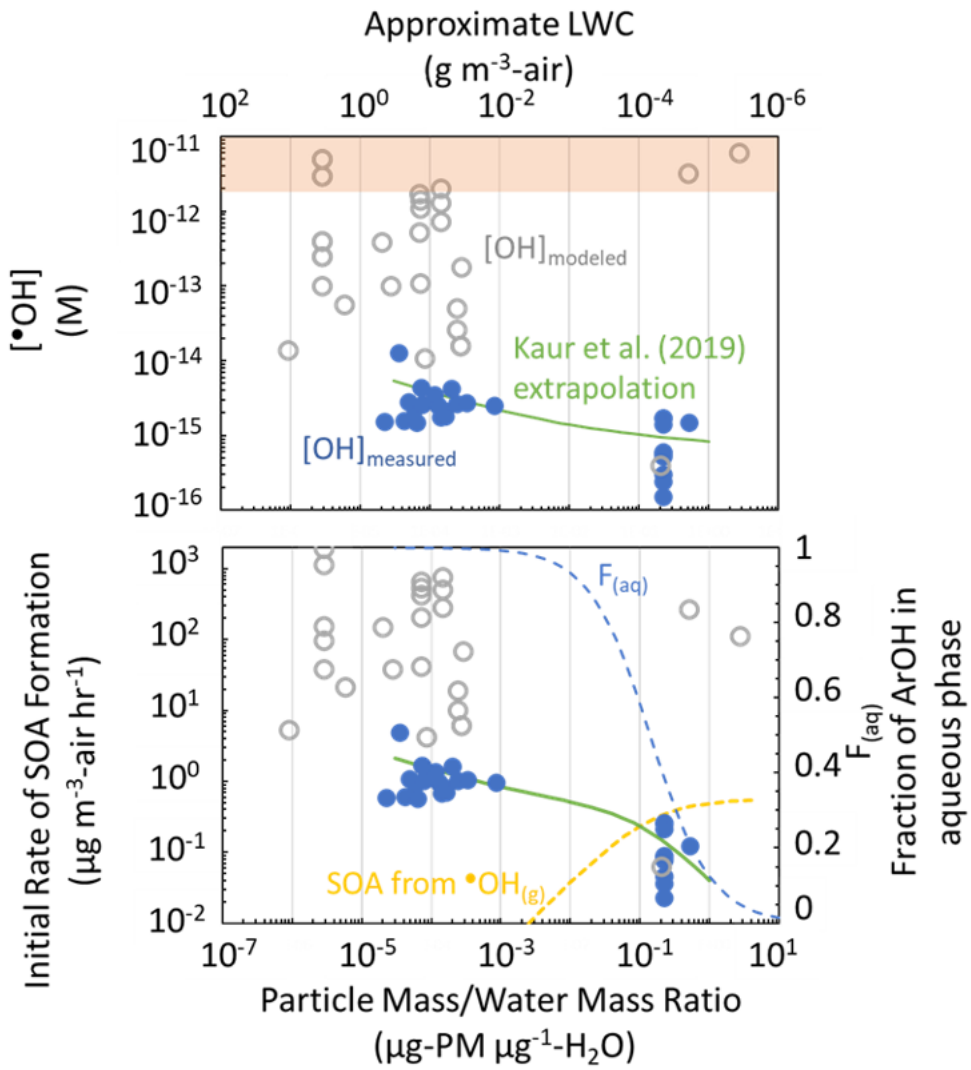

Figure 5. Top panel: Comparison of measured (blue circles) and modeled (gray circles) hydroxyl radical concentrations in fog drops, cloud drops, and aqueous particles; data sources and values are listed in Tables S7 and S8 and are plotted in Figure S8. Both measured and modeled data include calculated rates of gas-to-drop mass transport of gas-phase •OH. The green line represents the [•$OH_{(aq)}$] extrapolation from Kaur et al. (2019) for extracts of winter particles from Davis, CA.[24] The orange box represents •OH concentrations calculated assuming Henry's Law equilibrium with gas-phase •OH concentrations from the modeling studies, $(1.3 – 7.4) \times 10^6$ molecules cm^{-3},[76–81] and a Henry's law constant of 38.5 M atm^{-1}.[82] Bottom panel: Initial rate of SOA formation from the oxidation of syringyl acetone (SA) by gas- and aqueous-•OH in an air parcel containing a total of 5 µg m^{-3} syringyl acetone that is partitioned according to Henry's law at the specified particle mass/water mass ratio. The dashed blue line represents the fraction of SA

present in the aqueous phase, assuming Henry's law equilibrium. The points represent rates of aqSOA formation calculated based on the measured or modeled aqueous $^{\bullet}OH$ concentration from the top panel and the aqueous SA concentration at a given LWC. The green curve represents calculated rates of aqSOA formation based on the $^{\bullet}OH$ concentration extrapolation from Kaur et al.[24] The dotted yellow line is the rate of gas-phase SOA formation from $^{\bullet}OH_{(g)}$ reaction with syringyl acetone, assuming a gas-phase $^{\bullet}OH$ concentration of 1×10^{6} cm^{-3}.

References

(1) Shiraiwa, M.; Ueda, K.; Pozzer, A.; Lammel, G.; Kampf, C. J.; Fushimi, A.; Enami, S.; Arangio, A. M.; Fröhlich-Nowoisky, J.; Fujitani, Y.; Furuyama, A; Laker, P. S. J.; Lelieveld, J.; Lucas, K.; Morino, Y.; Pöschl, U.; Takahama, S.; Takami, A.; Tong, H.; Weber, B.; Yoshino, A.; Sato, K. Aerosol Health Effects from Molecular to Global Scales. *Environ. Sci. Technol.* **2017**, *51*, 13545–13567.

(2) Brey, S. J.; Barnes, E. A.; Pierce, J. R.; Wiedinmyer, C.; Fischer, E. V. Environmental conditions, ignition type, and air quality impacts of wildfires in the southeastern and western united states. *Earths Future* **2018**, *6*, 1442–1456.

(3) Voulgarakis, A.; Marlier, M. E.; Faluvegi, G.; Shindell, D. T.; Tsigaridis, K.; Mangeon, S. Interannual variability of tropospheric trace gases and aerosols: The role of biomass burning emissions. *J. Geophys. Res. Atmos.* **2015**, *120*, 7157–7173.

(4) Naeher, L. P.; Brauer, M.; Lipsett, M.; Zelikoff, J. T.; Simpson, C. D.; Koenig, J. Q.; Smith, K. R. Woodsmoke health effects: a review. *Inhal. Toxicol.* **2007**, *19*, 67–106.

(5) Zhang, Q.; Jimenez, J. L.; Canagaratna, M. R.; Allan, J. D.; Coe, H.; Ulbrich, I.; Alfarra, M. R.; Takami, A.; Middlebrook, A. M.; Sun, Y. L.; Dzepina, K.; Dunlea, E.; Docherty, K.; DeCarlo, P. F.; Salcedo, D.; Onasch, T.; Jayne, J. T.; Miyoshi, T.; Shimono, A.; Hatakeyama, S.; Takegawa, N.; Kondo, Y.; Schneider, J.; Drewnick, F.; Borrmann, S.; Weimer, S.; Demerjian, K.; Williams, P.; Bower, K.; Bahreini, R.; Cottrell, L.; Griffin, R. J.; Rautiainen, J.; Sun, J. Y.; Zhang, Y. M.; Worsnop, D. R. Ubiquity and dominance of oxygenated species in organic aerosols in anthropogenically-influenced Northern Hemisphere midlatitudes. *Geophys. Res. Lett.* **2007**, *34*, L13801.

(6) Tuet, W. Y.; Chen, Y.; Fok, S.; Champion, J. A.; Ng, N. L. Inflammatory responses to secondary organic aerosols (SOA) generated from biogenic and anthropogenic precursors. *Atmos. Chem. Phys.* **2017**, *17*, 11423–11440.

(7) Ervens, B.; Turpin, B. J.; Weber, R. J. Secondary organic aerosol formation in cloud droplets and aqueous particles (aqSOA): a review of laboratory, field and model studies. *Atmos. Chem. Phys.* **2011**, *11* (21), 11069–11102.

(8) McNeill, V. F. Aqueous organic chemistry in the atmosphere: sources and chemical processing of organic aerosols. *Environ. Sci. Technol.* **2015**, *49*, 1237–1244.

(9) Herrmann, H.; Schaefer, T.; Tilgner, A.; Styler, S. A.; Weller, C.; Teich, M.; Otto, T. Tropospheric aqueous-phase chemistry: kinetics, mechanisms, and its coupling to a changing gas phase. *Chem. Rev.* **2015**, *115*, 4259–4334.

(10) Lauraguais, A.; Coeur-Tourneur, C.; Cassez, A.; Deboudt, K.; Fourmentin, M.; Choël, M. Atmospheric reactivity of hydroxyl radicals with guaiacol (2-methoxyphenol), a

biomass burning emitted compound: Secondary organic aerosol formation and gas-phase oxidation products. *Atmos. Environ.* **2014**, *86*, 155–163.

(11) Lauraguais, A.; Coeur-Tourneur, C.; Cassez, A.; Seydi, A. Rate constant and secondary organic aerosol yields for the gas-phase reaction of hydroxyl radicals with syringol (2,6-dimethoxyphenol). *Atmos. Environ.* **2012**, *55*, 43–48.

(12) Smith, J. D.; Kinney, H.; Anastasio, C. Aqueous benzene-diols react with an organic triplet excited state and hydroxyl radical to form secondary organic aerosol. *Phys. Chem. Chem. Phys.* **2015**, *17*, 10227–10237.

(13) Oros, D. R.; Simoneit, B. R. T. Identification and emission factors of molecular tracers in organic aerosols from biomass burning Part 1. Temperate climate conifers. *Appl. Geochem.* **2001**, *16*, 1513–1544.

(14) Schauer, J. J.; Kleeman, M. J.; Cass, G. R.; Simoneit, B. R. Measurement of emissions from air pollution sources. 3. C1-C29 organic compounds from fireplace combustion of wood. *Environ. Sci. Technol.* **2001**, *35*, 1716–1728.

(15) Simoneit, B. R. T. Biomass burning — a review of organic tracers for smoke from incomplete combustion. *Appl. Geochem.* **2002**, *17*, 129–162.

(16) Andreae, M. O. Emission of trace gases and aerosols from biomass burning – an updated assessment. *Atmos. Chem. Phys.* **2019**, *19*, 8523–8546.

(17) Yee, L. D.; Kautzman, K. E.; Loza, C. L.; Schilling, K. A.; Coggon, M. M.; Chhabra, P. S.; Chan, M. N.; Chan, A. W. H.; Hersey, S. P.; Crounse, J. D.; Wennberg, P. O.; Flagan, R. C.; Seinfeld, J. H. Secondary organic aerosol formation from biomass burning intermediates: phenol and methoxyphenols. *Atmos. Chem. Phys.* **2013**, *13*, 8019–8043.

(18) Canonica, S.; Hellrung, B.; Wirz, J. Oxidation of phenols by triplet aromatic ketones in aqueous solution. *J. Phys. Chem. A* **2000**, *104*, 1226–1232.

(19) Bhosale, G. S.; Vaidya, P. D.; Joshi, J. B.; Patil, R. N. Kinetics of ozonation of phenol and substituted phenols. *Ind. Eng. Chem. Res.* **2019**, *58*, 7461–7466.

(20) Herrmann, H.; Hoffmann, D.; Schaefer, T.; Bräuer, P.; Tilgner, A. Tropospheric aqueous-phase free-radical chemistry: radical sources, spectra, reaction kinetics and prediction tools. *ChemPhysChem* **2010**, *11*, 3796–3822.

(21) Lim, Y. B.; Tan, Y.; Perri, M. J.; Seitzinger, S. P.; Turpin, B. J. Aqueous chemistry and its role in secondary organic aerosol (SOA) formation. *Atmos. Chem. Phys.* **2010**, *10*, 10521–10539.

(22) Seinfeld, J. H.; Pankow, J. F. Organic atmospheric particulate material. *Annu. Rev. Phys. Chem.* **2003**, *54*, 121–140.

(23) Appiani, E.; McNeill, K. Photochemical production of singlet oxygen from particulate organic matter. *Environ. Sci. Technol.* **2015**, *49*, 3514–3522.

(24) Kaur, R.; Labins, J. R.; Helbock, S. S.; Jiang, W.; Bein, K. J.; Zhang, Q.; Anastasio, C. Photooxidants from brown carbon and other chromophores in illuminated particle extracts. *Atmos. Chem. Phys.* **2019**, *19*, 6579–6594.

(25) Arakaki, T.; Faust, B. C. Sources, sinks, and mechanisms of hydroxyl radical ($^{\bullet}$OH) photoproduction and consumption in authentic acidic continental cloud waters from Whiteface Mountain, New York: The role of the Fe(r) (r = II, III) photochemical cycle. *J. Geophys. Res.* **1998**, *103*, 3487–3504.

(26) Arakaki, T.; Anastasio, C.; Kuroki, Y.; Nakajima, H.; Okada, K.; Kotani, Y.; Handa, D.; Azechi, S.; Kimura, T.; Tsuhako, A.; Miyagi, Y. A general scavenging rate constant for reaction of hydroxyl radical with organic carbon in atmospheric waters. *Environ. Sci. Technol.* **2013**, *47*, 8196–8203.

(27) Tilgner, A.; Herrmann, H. Tropospheric Aqueous-Phase OH Oxidation Chemistry: Current Understanding, Uptake of Highly Oxidized Organics and Its Effects. In *Multiphase environmental chemistry in the atmosphere*; Hunt, S. W.; Laskin, A.; Nizkorodov, S. A., Eds.; ACS Symposium Series; American Chemical Society: Washington, DC, 2018; Vol. 1299, pp. 49–85.

(28) Scully, F. E.; Hoigné, J. Rate constants for reactions of singlet oxygen with phenols and other compounds in water. *Chemosphere* **1987**, *16*, 681–694.

(29) Nakao, S.; Clark, C.; Tang, P.; Sato, K.; Cocker III, D. Secondary organic aerosol formation from phenolic compounds in the absence of NO_x. *Atmos. Chem. Phys.* **2011**, *11*, 10649–10660.

(30) Ma, L.; Guzman, C.; Niedek, C.; Tran, T.; Zhang, Q.; Anastasio, C. Kinetics and Mass Yields of Aqueous Secondary Organic Aerosol from Highly Substituted Phenols Reacting with a Triplet Excited State. *Environ. Sci. Technol.* **2021**, *55*, 5772-5781.

(31) Yu, L.; Smith, J.; Laskin, A.; George, K. M.; Anastasio, C.; Laskin, J.; Dillner, A. M.; Zhang, Q. Molecular transformations of phenolic SOA during photochemical aging in the aqueous phase: competition among oligomerization, functionalization, and fragmentation. *Atmos. Chem. Phys.* **2016**, *16*, 4511–4527.

(32) Anastasio, C.; Newberg, J. T. Sources and sinks of hydroxyl radical in sea-salt particles. *J. Geophys. Res. Atmos.* **2007**, *112* (D10), D10306.

(33) Sagebiel, J. C.; Seiber, J. N.; Woodrow, J. E. Comparison of headspace and gas-stripping methods for determining the Henry's law constant (H) for organic compounds of low to intermediate H. *Chemosphere* **1992**, *25*, 1763–1768.

(34) Feigenbrugel, V.; Le Calvé, S.; Mirabel, P.; Louis, F. Henry's law constant measurements for phenol, o-, m-, and p-cresol as a function of temperature. *Atmos. Environ.* **2004**, *38*, 5577–5588.

(35) McFall, A. S.; Johnson, A. W.; Anastasio, C. Air-Water Partitioning of Biomass-Burning Phenols and the Effects of Temperature and Salinity. *Environ. Sci. Technol.* **2020**, *54*, 3823–3830.

(36) Herrmann, H. Kinetics of aqueous phase reactions relevant for atmospheric chemistry. *Chem. Rev.* **2003**, *103*, 4691–4716.

(37) Parworth, C. L.; Young, D. E.; Kim, H.; Zhang, X.; Cappa, C. D.; Collier, S.; Zhang, Q. Wintertime water-soluble aerosol composition and particle water content in Fresno, California. *J. Geophys. Res. Atmos.* **2017**, *122*, 3155–3170.

(38) Nguyen, T. K. V.; Zhang, Q.; Jimenez, J. L.; Pike, M.; Carlton, A. G. Liquid water: ubiquitous contributor to aerosol mass. *Environ. Sci. Technol. Lett.* **2016**, *3*, 257–263.

(39) Smith, J. D.; Kinney, H.; Anastasio, C. Phenolic carbonyls undergo rapid aqueous photodegradation to form low-volatility, light-absorbing products. *Atmos. Environ.* **2016**, *126*, 36–44.

(40) Faust, J. A.; Wong, J. P. S.; Lee, A. K. Y.; Abbatt, J. P. D. Role of Aerosol Liquid Water in Secondary Organic Aerosol Formation from Volatile Organic Compounds. *Environ. Sci. Technol.* **2017**, *51*, 1405–1413.

(41) Mekic, M.; Gligorovski, S. Ionic strength effects on heterogeneous and multiphase chemistry: Clouds versus aerosol particles. *Atmos. Environ.* **2021**, *244*, 117911.

(42) Zhou, W.; Mekic, M.; Liu, J.; Loisel, G.; Jin, B.; Vione, D.; Gligorovski, S. Ionic strength effects on the photochemical degradation of acetosyringone in atmospheric deliquescent aerosol particles. *Atmos. Environ.* **2019**, *198*, 83–88.

(43) Loisel, G.; Mekic, M.; Liu, S.; Song, W.; Jiang, B.; Wang, Y.; Deng, H.; Gligorovski, S. Ionic strength effect on the formation of organonitrate compounds through photochemical degradation of vanillin in liquid water of aerosols. *Atmos. Environ.* **2021**, *246*, 118140.

(44) Miller, W. L.; Kester, D. R. Hydrogen peroxide measurement in seawater by (p-hydroxyphenyl)acetic acid dimerization. *Anal. Chem.* **1988**, *60*, 2711–2715.

(45) Anastasio, C.; McGregor, K. G. Chemistry of fog waters in California's Central Valley: 1. In situ photoformation of hydroxyl radical and singlet molecular oxygen. *Atmos. Environ.* **2001**, *35*, 1079–1089.

(46) Galbavy, E. S.; Ram, K.; Anastasio, C. 2-Nitrobenzaldehyde as a chemical actinometer for solution and ice photochemistry. *J. Photochem. Photobiol. A* **2010**, *209*, 186–192.

(47) Sun, Y. L.; Zhang, Q.; Anastasio, C.; Sun, J. Insights into secondary organic aerosol formed via aqueous-phase reactions of phenolic compounds based on high resolution mass spectrometry. *Atmos. Chem. Phys.* **2010**, *10*, 4809–4822.

(48) Yu, L.; Smith, J.; Laskin, A.; Anastasio, C.; Laskin, J.; Zhang, Q. Chemical characterization of SOA formed from aqueous-phase reactions of phenols with the triplet excited state of carbonyl and hydroxyl radical. *Atmos. Chem. Phys.* **2014**, *14*, 13801–13816.

(49) Lauraguais, A.; Bejan, I.; Barnes, I.; Wiesen, P.; Coeur, C. Rate Coefficients for the Gas-Phase Reactions of Hydroxyl Radicals with a Series of Methoxylated Aromatic Compounds. *J. Phys. Chem. A* **2015**, *119*, 6179–6187.

(50) Ragnar, M.; Lindgren, C. T.; Nilvebrant, N.-O. pK_a -Values of Guaiacyl and Syringyl Phenols Related to Lignin. *Journal of Wood Chemistry and Technology* **2000**, *20*, 277–305.

(51) Erdemgil, F. Z.; Sanli, S.; Sanli, N.; Ozkan, G.; Barbosa, J.; Guiteras, J.; Beltrán, J. L. Determination of pK(a) values of some hydroxylated benzoic acids in methanol-water binary mixtures by LC methodology and potentiometry. *Talanta* **2007**, *72*, 489–496.

(52) Kroflič, A.; Anders, J.; Drventić, I.; Mettke, P.; Böge, O.; Mutzel, A.; Kleffmann, J.; Herrmann, H. Guaiacol Nitration in a Simulated Atmospheric Aerosol with an Emphasis on Atmospheric Nitrophenol Formation Mechanisms. *ACS Earth Space Chem.* **2021**, *5*, 1083-1093.

(53) Simoneit, B. R. T.; Schauer, J. J.; Nolte, C. G.; Oros, D. R.; Elias, V. O.; Fraser, M. P.; Rogge, W. F.; Cass, G. R. Levoglucosan, a tracer for cellulose in biomass burning and atmospheric particles. *Atmos. Environ.* **1999**, *33*, 173–182.

(54) Deguillaume, L.; Leriche, M.; Monod, A.; Chaumerliac, N. The role of transition metal ions on HO_x radicals in clouds: a numerical evaluation of its impact on multiphase chemistry. *Atmos. Chem. Phys.* **2004**, *4*, 95–110.

(55) Deguillaume, L.; Leriche, M.; Desboeufs, K.; Mailhot, G.; George, C.; Chaumerliac, N. Transition metals in atmospheric liquid phases: sources, reactivity, and sensitive parameters. *Chem. Rev.* **2005**, *105*, 3388–3431.

(56) Brezonik, P. L.; Fulkerson-Brekken, J. Nitrate-Induced Photolysis in Natural Waters: Controls on Concentrations of Hydroxyl Radical Photo-Intermediates by Natural Scavenging Agents. *Environ. Sci. Technol.* **1998**, *32*, 3004–3010.

(57) Huang, D. D.; Zhang, Q.; Cheung, H. H. Y.; Yu, L.; Zhou, S.; Anastasio, C.; Smith, J. D.; Chan, C. K. Formation and Evolution of aqSOA from Aqueous-Phase Reactions of Phenolic Carbonyls: Comparison between Ammonium Sulfate and Ammonium Nitrate Solutions. *Environ. Sci. Technol.* **2018**, *52*, 9215–9224.

(58) Bucknall, T.; Edwards, H. E.; Kemsley, K. G.; Moore, J. S.; Phillips, G. O. The formation of malonaldehyde in irradiated carbohydrates. *Carbohydr. Res.* **1978**, *62*, 49–59.

(59) Chen, Z.; Chu, L.; Galbavy, E. S.; Ram, K.; Anastasio, C. Hydroxyl radical in/on illuminated polar snow: formation rates, lifetimes, and steady-state concentrations. *Atmos. Chem. Phys.* **2016**, *16*, 9579–9590.

(60) Feng, W.; Nansheng, D. Photochemistry of hydrolytic iron (III) species and photoinduced degradation of organic compounds. A minireview. *Chemosphere* **2000**, *41*, 1137–1147.

(61) Pang, H.; Zhang, Q.; Wang, H.; Cai, D.; Ma, Y.; Li, L.; Li, K.; Lu, X.; Chen, H.; Yang, X.; Chen, J. Photochemical Aging of Guaiacol by Fe(III)-Oxalate Complexes in Atmospheric Aqueous Phase. *Environ. Sci. Technol.* **2019**, *53*, 127–136.

(62) Jung, Y. S.; Lim, W. T.; Park, J.-Y.; Kim, Y.-H. Effect of pH on Fenton and Fenton-like oxidation. *Environ. Technol.* **2009**, *30*, 183–190.

(63) Lu, H.-F.; Chen, H.-F.; Kao, C.-L.; Chao, I.; Chen, H.-Y. A computational study of the Fenton reaction in different pH ranges. *Phys. Chem. Chem. Phys.* **2018**, *20*, 22890–22901.

(64) Qin, H.; Fan, J.; Mao, S. Exploring the mechanism of the Fe(iii)-activated Fenton-like reaction based on a quantitative study. *New J. Chem.* **2020**, *44*, 8952–8959.

(65) Hayyan, M.; Hashim, M. A.; AlNashef, I. M. Superoxide ion: generation and chemical implications. *Chem. Rev.* **2016**, *116*, 3029–3085.

(66) Bielski, B. H. J.; Cabelli, D. E.; Arudi, R. L.; Ross, A. B. Reactivity of HO_2 /O_2^- radicals in aqueous solution. *J. Phys. Chem. Ref. Data* **1985**, *14*, 1041–1100.

(67) Rabani, J.; Klug-Roth, D.; Lilie, J. Pulse radiolytic investigations of the catalyzed disproportionation of peroxy radicals. Aqueous cupric ions. *J. Phys. Chem.* **1973**, *77*, 1169–1175.

(68) Pan, Y.; Garg, S.; Waite, T. D.; Yang, X. Copper Inhibition of Triplet-Induced Reactions Involving Natural Organic Matter. *Environ. Sci. Technol.* **2018**, *52*, 2742–2750.

(69) Pan, Y.; Ruan, X.; Garg, S.; Waite, T. D.; Lei, Y.; Yang, X. Copper Inhibition of Triplet-Sensitized Phototransformation of Phenolic and Amine Contaminants. *Environ. Sci. Technol.* **2020**, *54*, 9980–9989.

(70) Mvula, E.; Schuchmann, M. N.; von Sonntag, C. Reactions of phenol-OH-adduct radicals. Phenoxyl radical formation by water elimination vs. oxidation by dioxygen. *J. Chem. Soc., Perkin Trans. 2* **2001**, 264–268.

(71) Ahern, A. T.; Robinson, E. S.; Tkacik, D. S.; Saleh, R.; Hatch, L. E.; Barsanti, K. C.; Stockwell, C. E.; Yokelson, R. J.; Presto, A. A.; Robinson, A. L.; Sullivan, R. C.; Donahue, N. M. Production of secondary organic aerosol during aging of biomass burning smoke from fresh fuels and its relationship to VOC precursors. *J. Geophys. Res. Atmos.* **2019**, *124*, 3583–3606.

(72) Lim, C. Y.; Hagan, D. H.; Coggon, M. M.; Koss, A. R.; Sekimoto, K.; Gouw, J. de; Warneke, C.; Cappa, C. D.; Kroll, J. H. Secondary organic aerosol formation from the laboratory oxidation of biomass burning emissions. *Atmos. Chem. Phys.* **2019**, *19*, 12797–12809.

(73) Gilardoni, S.; Massoli, P.; Paglione, M.; Giulianelli, L.; Carbone, C.; Rinaldi, M.; Decesari, S.; Sandrini, S.; Costabile, F.; Gobbi, G. P.; Pietrogrande, M. C.; Visentin, M.; Scotto, F.; Fuzzi, S.; Facchini, M. C. Direct observation of aqueous secondary organic aerosol from biomass-burning emissions. *Proc Natl Acad Sci USA* **2016**, *113*, 10013–10018.

(74) Hoffmann, E. H.; Tilgner, A.; Wolke, R.; Böge, O.; Walter, A.; Herrmann, H. Oxidation of substituted aromatic hydrocarbons in the tropospheric aqueous phase: kinetic mechanism development and modelling. *Phys. Chem. Chem. Phys.* **2018**, *20*, 10960–10977.

(75) Schauer, J. J.; Cass, G. R. Source Apportionment of Wintertime Gas-Phase and Particle-Phase Air Pollutants Using Organic Compounds as Tracers. *Environ. Sci. Technol.* **2000**, *34*, 1821–1832.

(76) Ervens, B.; Volkamer, R. Glyoxal processing by aerosol multiphase chemistry: towards a kinetic modeling framework of secondary organic aerosol formation in aqueous particles. *Atmos. Chem. Phys.* **2010**, *10*, 8219–8244.

(77) Ervens, B.; Sorooshian, A.; Lim, Y. B.; Turpin, B. J. Key parameters controlling OH-initiated formation of secondary organic aerosol in the aqueous phase (aqSOA). *J. Geophys. Res. Atmos.* **2014**, *119*, 3997–4016.

(78) Jacob, D. J.; Gottlieb, E. W.; Prather, M. J. Chemistry of a polluted cloudy boundary layer. *J. Geophys. Res. Atmos.* **1989**, *94*, 12975–13002.

(79) Pandis, S. N.; Seinfeld, J. H. Sensitivity analysis of a chemical mechanism for aqueous-phase atmospheric chemistry. *J. Geophys. Res. Atmos.* **1989**, *94*, 1105–1126.

(80) Warneck, P. In-cloud chemistry opens pathway to the formation of oxalic acid in the marine atmosphere. *Atmos. Environ.* **2003**, *37*, 2423–2427.

(81) Warneck, P. Multi-Phase Chemistry of C2 and C3 Organic Compounds in the Marine Atmosphere. *J. Atmos. Chem.* **2005**, *51*, 119–159.

(82) Sander, R. Compilation of Henry's law constants (version 4.0) for water as solvent. *Atmos. Chem. Phys.* **2015**, *15*, 4399–4981.

Supplemental Information for

Aqueous •OH Oxidation of Highly Substituted Phenols as a Source of Secondary Organic Aerosol

Stephanie Arciva[1], Christopher Niedek[2], Camille Mavis[1], Melanie Yoon[1], Martin Esparza Sanchez[1], Qi Zhang[2], and Cort Anastasio[1]

[1]Department of Land, Air, and Water Resource, University of California, Davis, CA 95616

[2]Department of Environmental Toxicology, University of California, Davis, CA 95616

Correspondence to: Cort Anastasio (canastasio@ucdavis.edu)

Submitted to Environmental Science & Technology, 3/29/22

This Supporting Information contains 27 pages and includes 5 text sections, 8 figures, and 8 tables.

Table of Contents

Section S1: Individual kinetic experiments

Second-order rate constants were determined as the average of 3 or 4 individual experiments. Unknown rate constants for ArOH test compounds were determined by multiplying the experimental ratio of the pseudo-first-order rate constants of the test and reference ArOH, k'_{test}/k'_{ref}, by the known second-order rate constant of the reference compound with •OH (equation 1, main text). Values of reference rate constants are in Table S3.

Table S1: Individual kinetic experiments

Test Compound	pH	Ratio ($\frac{k'_{test}}{k'_{ref}}$)	Second order rate constant (10^9 M^{-1} s^{-1})
Tyrosol[a] 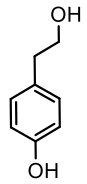	2	0.969	1.9
		0.950	1.9
		0.935	1.9
	5	0.999	15.0
		1.094	13.7
		1.093	13.7
Vanillyl alcohol[b] 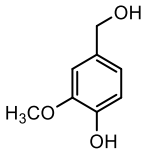	2	1.08	7.3
		1.33	9.0
		1.21	8.2
	5	1.04	16.6
		1.02	16.4
		1.02	16.3
Guaiacylacetone[b] 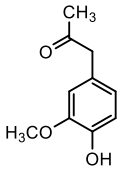	2	0.91	7.4
		0.65	10.5
		0.80	8.5
		0.71	9.6
	5	1.098	14.6
		1.089	14.7
		1.109	14.4
		1.02	15.7
Syringyl acetone[b]	2	0.92	13.7
		0.95	14.3
		0.97	14.6

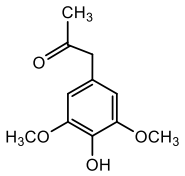	5	1.54 1.51 1.55	24.6 24.2 24.8
trans/*cis*- Ferulic acid[b]	2	1.82 1.89 1.89	12.4 12.9 12.9
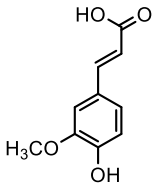 (*trans*-Ferulic acid)	6	1.18 1.21 1.14	18.9 19.4 18.2
Syringic acid[b]	2	1.29 1.44 1.60 1.19	8.78 9.76 10.9 8.1
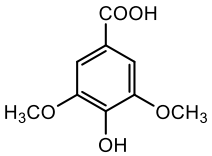	6	1.17 1.29 1.18 1.31	20.9 18.8 18.9 20.6

[a] Second-order rate constants determined by using a relative rate method with phenol as a reference compound.

[b] Second-order rate constants determined by using a relative rate method with guaiacol as a reference compound.

753

754

755

756 **Table S2:** HPLC methods used to quantify ArOH concentrations. All methods used an eluent
757 flow rate of 0.6 mL min^{-1}. HPLC instrumentation: Shimadzu LC-10AT pump, ThermoScientific
758 BetaBasic-18 C_{18} column (250 × 3mm, 5 μm bead), and Shimadzu-10AT UV-Vis detector

Compound	Eluent (Vol:Vol)	Detection wavelength (nm)
Tyrosol	20%:80% ACN [a]: H_2O	280
Vanillyl alcohol	20%:80% ACN: H_2O	280
Guaiacylacetone	20%:80% ACN: H_2O	280
Ferulic acid	20%:80% ACN: 2% acetic acid in H_2O	320
Syringic acid	20%:80% ACN: 2% acetic acid in H_2O	280
Syringylacetone	15%:85% ACN: H_2O	280

759 [a] ACN = acetonitrile

760

761

762

763

764

765

766

767

768

769

770

771

772

773

774

775 **Section S2: Direct photodegradation and photoisomerization of ArOH**

776 Syringic acid (SyrAcid), syringyl acetone (SA), and ferulic acid (FA) undergo direct
777 photodegradation. On the same day of a given ArOH-$^{\bullet}$OH oxidation experiment, we also measured
778 the direct photodegradation of the same ArOH by preparing a pH-adjusted solution of 15 μM
779 ArOH (the same concentration as oxidation experiments) without the addition of H_2O_2. We
780 measured ArOH photodecay at the same time intervals as the oxidation experiment, enabling us to
781 directly subtract ArOH direct photodegradation from the phenol decay in the oxidation experiment,
782 yielding a rate constant representative of $^{\bullet}$OH oxidation alone. Direct photodegradation was
783 slowest for ferulic acid, with a rate constant of 2.1×10^{-6} s^{-1}. Syringol-based compounds undergo
784 faster direct photodegradation, with j_{ArOH} values of 6.6×10^{-5} s^{-1} for syringic acid and 2.8×10^{-5} s^{-}
785 ^{1} for syringyl acetone. $^{\bullet}$OH rate constants in the main text represent final rate constants with
786 photodegradation corrections.

787 Ferulic acid also undergoes rapid *cis*/*trans* photoisomerization, reaching a photo-stationary state
788 within 3 min in our illumination system.[1] To allow for photoisomerization to occur before starting
789 our $^{\bullet}$OH kinetic determination, we illuminated pH-adjusted solutions containing 15 μM *trans*-
790 ferulic acid for 10 min to achieve the isomerization steady state, spiked with 10 mM H_2O_2, then
791 proceeded with the oxidation experiment.

792

Table S3: Second-order rate constants for reactions of reference compounds with •OH. For each reference compound we used the average rate constant (which was determined using all values here) in our calculations.

Reference Compound	$k_{Reference + \bullet OH}$ (10^9 M^{-1} s^{-1})			
	pH 2	**Reference**	**pH 5**	**Reference**
Phenol	2.0 (±0.2)	Smith et al. 2015[2]	18.5 (±0.5)	Smith et al. 2015[2]
	1.8 (±0.2)	Smith et al. 2015[2]	9.0 (±0.5)	Smith et al. 2015[2]
	1.9 (±0.2)	Hermann et al. 2010[3]	18	Ross et al. 1977[4]
	2.1	Field et al. 1982[5]	11	Ross et al. 1977[4]
			14	Land et al. 1967[6]
Avg (± 1σ)	2.0 (±0.1)		14 (±4)	
Guaiacol	4.5 (±0.2)	Smith et al. 2015[2]	18 (±0.5)	Smith et al. 2015[2]
	9.0 (±2)	Smith et al. 2015[2]	21 (±0.8)	Smith et al. 2015[2]
	5.2 (±0.05)[a]	This work	12 (±0.4)	Smith et al. 2015[2]
	11 (±0.08)[b]	This work	15	Steenken and O'Neill 1977[7]
			11 (±0.01)	He et al. 2019[8]
Avg (± 1σ)	7.4 (±3.1)		14 (±4)	
Syringol	16 (±2)	Smith et al. 2015[2]	21 (±0.8)	Smith et al. 2015[2]
	12 (±6)	Smith et al. 2015[2]	18 (±0.5)	Smith et al. 2015[2]
	23 (±0.5)[a]	This work	14 (±4)	Smith et al. 2015[2]
	25 (±0.4)[a]	This work	18 (±4)	Steenken and O'Neill 1977[7]
			17 (±0.1)	He et al. 2019[8]
Avg (± 1σ)	19 (±6)		18 (±3)	

Reported error for each study represents the standard error. Error reported in average values from this work represent one standard deviation.

[a] Second-order rate constants determined by using a relative rate method with phenol as a reference compound (k = 2.0 x 10^9 M^{-1} s^{-1}) at pH 2, determined as the average of the four values in this table.

[b] Second-order rate constants determined by using a relative rate method with benzoic acid as a reference compound (k = 5.9 x 10^9 M^{-1} s^{-1} at pH 2).[7]

808 **Table S4:** Average (± 1σ) second-order rate constants for reactions of test compounds with •OH.
809 Each reported value was determined from 3 to 4 individual experiments. The error represents one
810 standard deviation, determined from the average of the individual experiments.

	$k_{Test + \bullet OH}$ (10^9 M^{-1} s^{-1})	
	pH 2	**pH 5**
Tyrosol	1.9 (±0.3)	14 (±5)
Guaiacylacetone	8.8 (±4.2)	15 (±5)
Vanillyl alcohol	8.2 (±3.8)	16 (±5)
Syringyl acetone	14 (±7)	25 (±8)
	pH 2	**pH 6**
***trans*-Ferulic acid**	13 (±6)	19 (±6) [a]
***cis*-Ferulic acid**	12 (±6)	19 (±6)
Syringic acid	9.4 (±4.4)	20 (±6)

811 [a] Our experimentally determined rate constant for *trans*-ferulic acid was 12 (±4) x 10^9 M^{-1} s^{-1}, but
812 we believe this is incorrectly slow because of coelution of trans-FA with FA-•OH oxidation
813 products on the HPLC. Because the timescale of photoisomerization for ferulic acid is much
814 more rapid than that of its reaction with •OH,[1] apparent rate constants for the two isomers with
815 •OH should be the same in our experiments. Thus we have assumed here the second-order rate
816 constant for *trans*-ferulic acid is the same as for the *cis* isomer.
817

818

Table S5: GA and GUA Oxidation Experiments at Various pH Values. Each reaction solution contained 10 μM GA, 10 μM GUA, the specified concentration of H_2O_2, and either sulfuric acid or sodium borate to adjust the pH. Solutions did not contain 2-propanol. We measured the pseudo-first-order rate constants for GA (k'_{GA}) and GUA (k'_{GUA}). We also measured the j_{2NB}, the photolysis of 2-nitrobenzaldehyde, our chemical actinometer. Data from this table are shown in Figure S1.

pH	$[H_2O_2]$ (mM)	j_{2NB} (10^{-2} s^{-1})	k'_{GA} (10^{-4} s^{-1})	k'_{GUA} (10^{-4} s^{-1})	k'_{GA} / k'_{GUA}
1.41	1.0	1.3	1.5	0.90	1.64
1.99	0.54	1.2	0.77	0.50	1.52
2.08	1.1	1.3	1.7	1.2	1.45
2.12	0.54	1.3	1.3	1.1	1.19
2.16	1.1	1.3	1.3	1.1	1.19
2.39	1.1	1.0	1.2	1.2	0.95
2.44	0.54	1.3	0.74	0.85	0.88
2.95	1.0	1.1	1.1	1.3	0.87
3.34	1.0	1.2	1.4	1.6	0.85
3.34	1.0	1.2	2.0	2.3	0.88
3.83	1.0	1.1	1.1	1.3	0.88
4.44	0.54	1.2	0.89	1.1	0.84
4.70	0.54	1.6	1.3	1.6	0.83
5.05	0.54	1.2	2.9	3.0	0.97
5.10	0.54	1.1	0.53	0.64	0.83

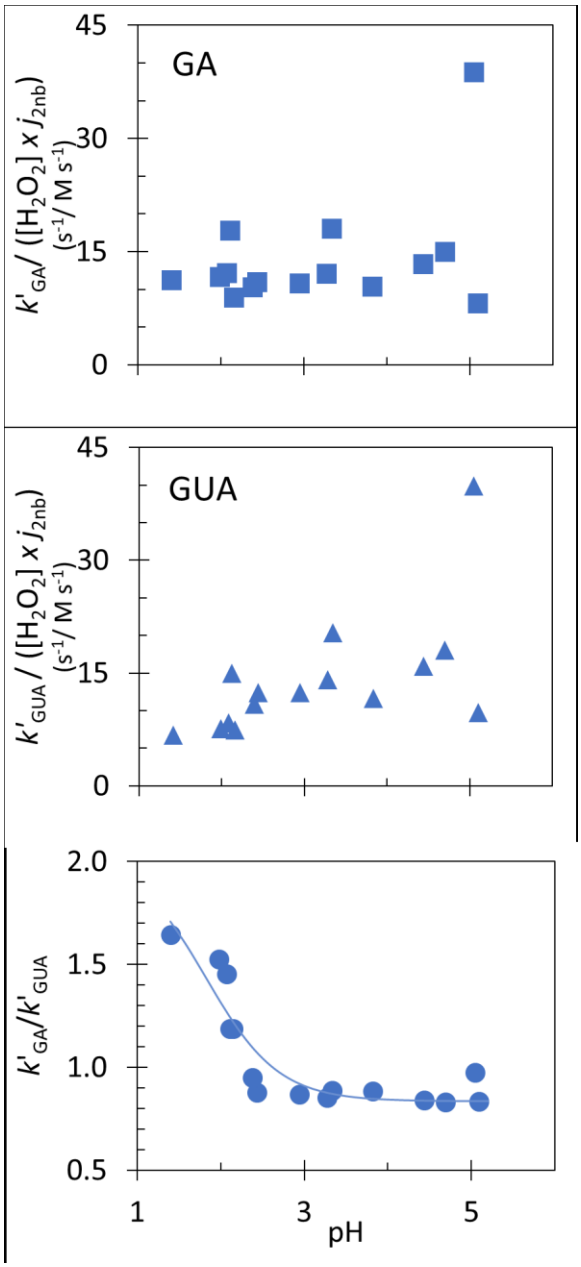

Figure S1: Top panel: Pseudo-first-order rate constants of guaiacylacetone (GA) loss in illuminated H_2O_2-containing solutions as a function of pH. Middle panel: Pseudo-first-order rate constants of guaiacol (GUA) in the same experiments. Bottom panel: The ratio of the pseudo-first-order rate constant of GA over GUA versus solution pH. The pH behavior was modeled by fitting the data to a three-parameter sigmoidal fit using Origin Pro. The blue line is the trendline fit: $\frac{k'_{GA}}{k'_{GUA}} = A + \frac{B-A}{1+\frac{[H^+]}{K_a}}$ with A = 2.03, B = 0.83, and K_a = 0.015 (R^2 = 0.86).

Section S3: Quantitative Structure Activity Relationships for ArOH rate constants and oxidation potentials

We developed quantitative structure activity relationships (QSARs) using oxidation potentials measured or modeled by Ma et al.[1] along with second-order rate constants for $^{\bullet}OH$ from this work (for highly substituted phenols) and from Smith et al. (for simple phenols).[2] Oxidation potentials for ArOH represent one-electron oxidation to form a radical cation, i.e., for the process $ArOH \rightarrow ArOH^{\bullet+} + e^{-}$.

ArOH oxidation potentials were measured using a three-electrode potentiostat consisting of a carbon working electrode, an Ag/AgCl KCl reference electrode, and a platinum counter electrode. Potentials were corrected from an Ag/AgCl reference electrode to the standard hydrogen electrode (SHE). Modeled oxidation potentials were calculated using Gaussian 09 software to derive the free energy of reaction (ΔG°_{ox}). One-electron oxidation potentials for ArOH were then calculated using SHE as the potential electrode. Details of oxidation potential measurements and modeling are in Ma et al.[1]

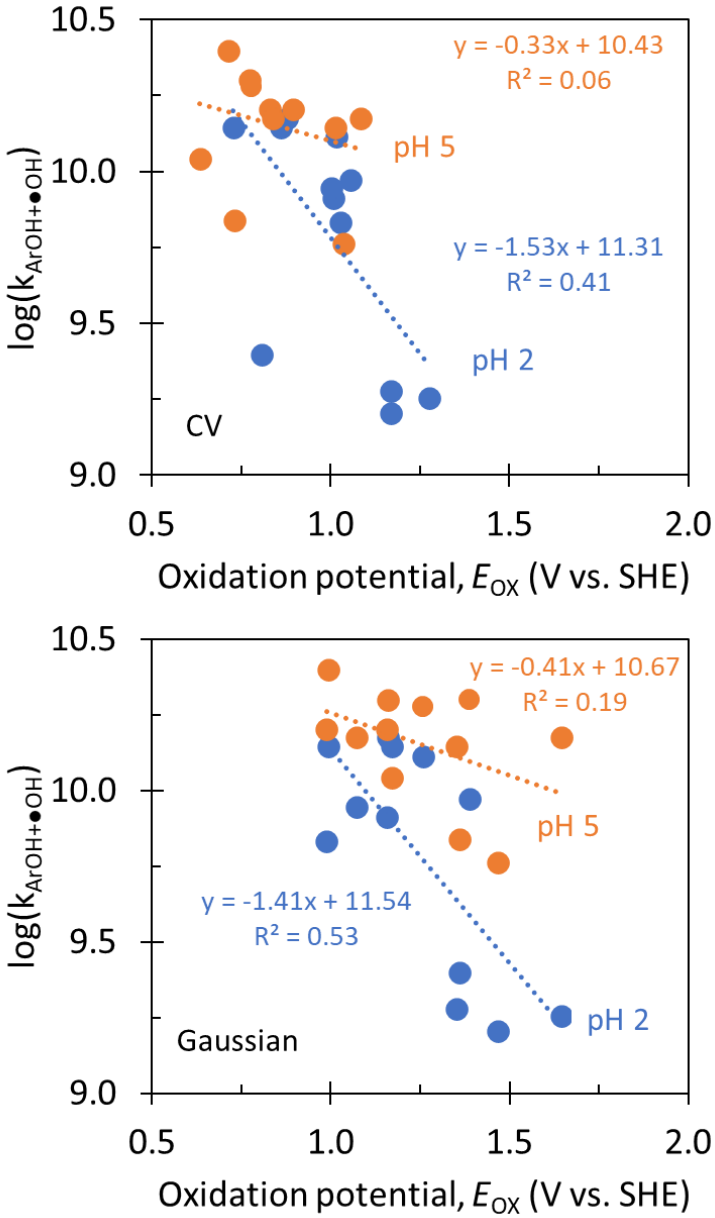

Figure S2: Quantitative structure activity relationship developed using second-order rate constants of phenols with $^{\bullet}$OH and oxidation potentials determined by Ma et al.[1] The top plot shows the QSAR based on oxidation potentials measured by cyclic voltammetry (CV) at pH 2 (blue) and pH 5 (orange). The bottom plot shows QSARs based on oxidation potentials calculated by Gaussian. Lines and equations represent the linear regression fits to each set of data.

859 **Table S6:** Oxidation potentials (E_{OX}) for the 12 phenols in the Figure S2 QSARs. Gaussian
860 values are modeled, while the CV values are measured using cyclic voltammetry.[1] Data
861 presented in Volts vs SHE. Rate constants are from this work and Smith et al.[2] for simple ArOH.

Compound	Gaussian E_{OX}	CV E_{OX}		$k_{ArOH+OH}$ (10^9 M^{-1} s^{-1})	
		pH 2	pH 5	pH 2	pH 5/6
Phenol	1.65	1.28	1.08	1.8	15
Guaiacol	0.99	1.03	0.89	6.8	16
Syringol	1.16	0.88	0.77	15	20
Catechol	1.36	0.81	0.73	2.5	6.9
Resorcinol	1.4	1.17	1.04	1.6	5.8
Hydroquinone	1.17	0.73	0.63	14	11
Tyrosol	1.35	1.17	1.01	1.9	14
Guaiacylacetone	1.07	1.00	0.84	8.8	15
Vanillyl alcohol	1.16	1.01	0.83	8.2	16
Ferulic acid	1.26	1.02	0.78	13	19
Syringic acid	1.39	1.06	0.78	9.4	20
Syringyl acetone	0.99	0.86	0.72	14	25

862

Section S4: aqSOA mass yields for highly substituted ArOH with •OH

Mass yields for the •OH-oxidation of highly substituted phenols were determined using aerosol mass spectrometry (AMS) as described previously.[1] Solutions containing 50 - 100 µM ArOH and 5 – 10 mM H_2O_2 were illuminated with simulated sunlight and aliquots were removed at $t_{1/2}$, $2t_{1/2}$, and $3t_{1/2}$, i.e., one, two and three half-lives for the phenol. Mass yields at each time point are shown in Figure S3, while average values for each phenol are reported in Figure 3 of the main paper. In determining the average mass yield for syringyl acetone, we removed the outlier at $3t_{1/2}$.

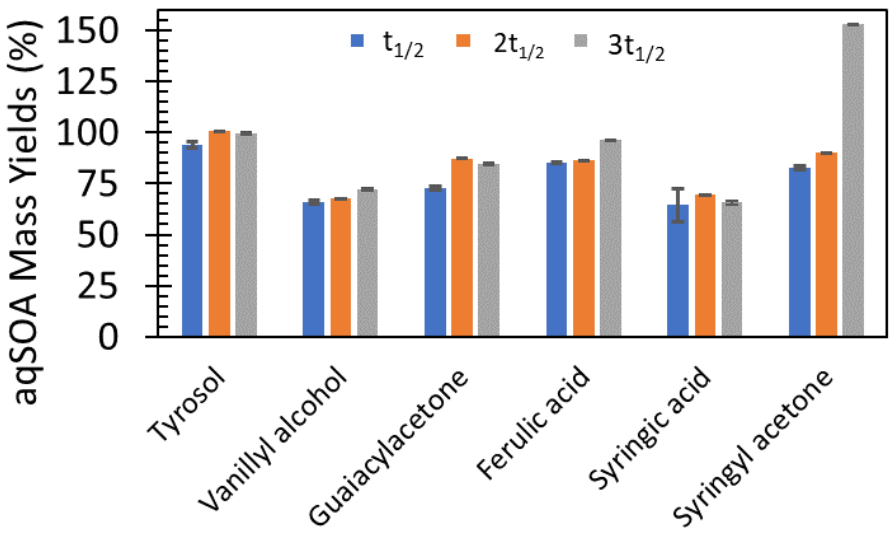

Figure S3: aqSOA mass yields determined from the illuminated solutions containing the test phenol and H_2O_2 at $t_{1/2}$, $2t_{1/2}$, and $3t_{1/2}$. For tyrosol, vanillyl alcohol, and guaiacylacetone, we ran experiments using 100 µM ArOH and 5 mM H_2O_2. For ferulic acid, syringic acid, and syringyl acetone, we ran experiments at 50 µM ArOH and 10 mM H_2O_2. Error bars are the standard deviations at each half-life, determined from duplicate samples. For each phenol's average we used results from each time point except for syringyl acetone, where the $3t_{1/2}$ point was not included in the average.

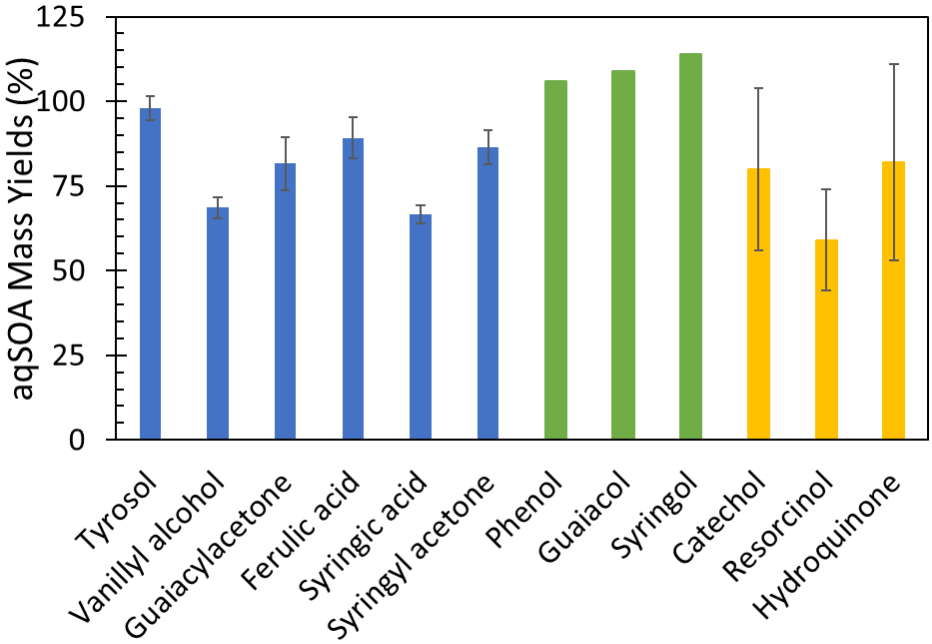

Figure S4: aqSOA mass yields for reactions of hydroxyl radical with: highly substituted phenols (blue; this work, measured using AMS), simple phenols from Yu et al.[8] (green; measured using AMS), and simple phenols from Smith et al.[2] (yellow; measured gravimetrically after using nitrogen gas to blow down each sample to dryness).

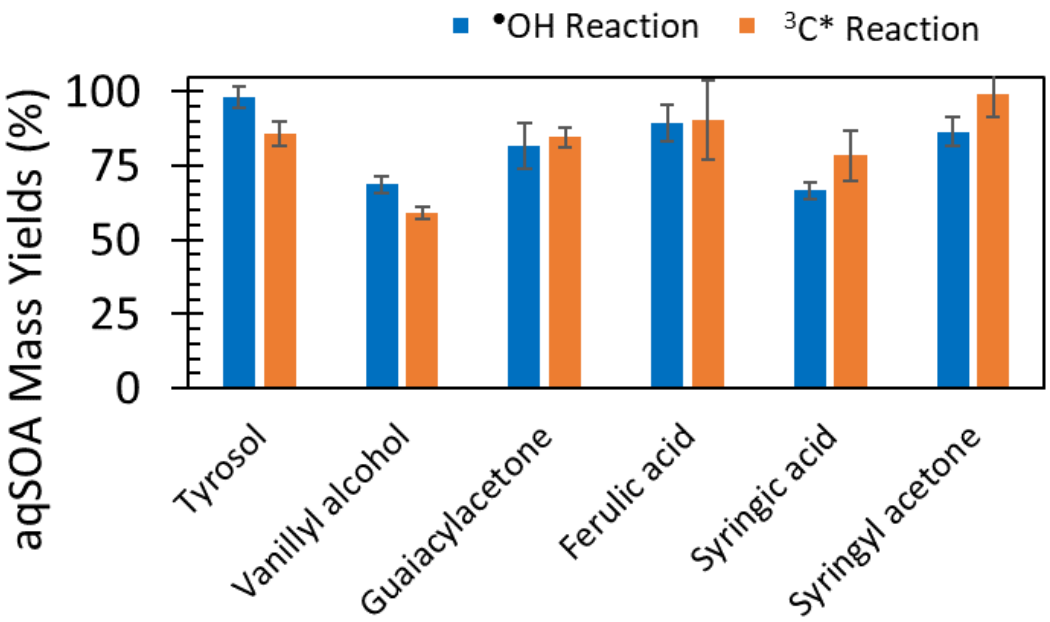

Figure S5: aqSOA mass yields determined using AMS for highly substituted phenols reacting with •OH (blue bars) or $^3C^*$ (orange bars; data from Ma et al.[1]). Error bars represent ± 1σ based on results from duplicate experiments.

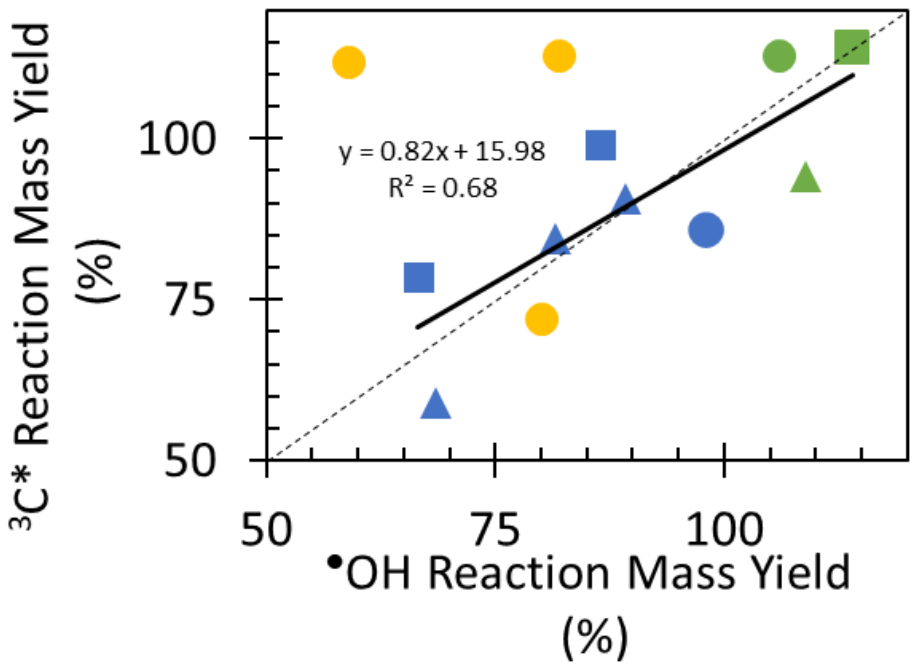

Figure S6: A comparison of aqSOA mass yields for phenols reacting with triplet excited states and hydroxyl radical. The blue symbols represent results for highly substituted phenols, where •OH data is from this work and $^3C^*$ data is from Ma et al..[1] The green symbols are aqSOA mass yields for phenol, guaiacol, and syringol,[9] while yellow symbols are data for catechol, resorcinol, and hydroquinone.[2] For all colors, circles represent C_6H_6OH-based compounds, triangles are guaiacol-based structures, and squares are syringol-based structures. The black dashed line is the 1:1 line, while the black solid line is the linear regression fit to blue and green data (highly substituted phenols from this study, and phenol, guaiacol, and syringol), with the regression function shown in black.

Section S5: Correction for internal light screening by ammonium nitrate

High concentrations of nitrate strongly absorb light near 300 nm, which reduces the average photon flux available for H_2O_2 photolysis. To correct for this internal light-screening by 500 mM NH_4NO_3, we determined a screening factor (S_λ):

$$S_\lambda = \frac{\sum[\left(1-10^{-\varepsilon_\lambda[C]l}\right)xI'_\lambda]}{\sum[(2.303x\varepsilon_\lambda[C]l)xI'_\lambda]}$$

In this equation, ε_λ is the molar absorptivity of ammonium nitrate at a given wavelength, [C] is the ammonium nitrate concentration, l is the pathlength of the illumination cell, and I'_λ is the photon flux of our illumination system at a given wavelength, previously determined in other work.[10] For our experiments examining the solute effect of nitrate (15 μM guaiacylacetone, 500 mM NH_4NO_3, 10 mM H_2O_2, 5 cm pathlength), we calculated $S_\lambda = 0.16$ for the wavelength region of 300 to 360 nm. We divided experimentally measured values of $k'_{GA,solute}$ by S_λ to estimate a corrected rate constant.

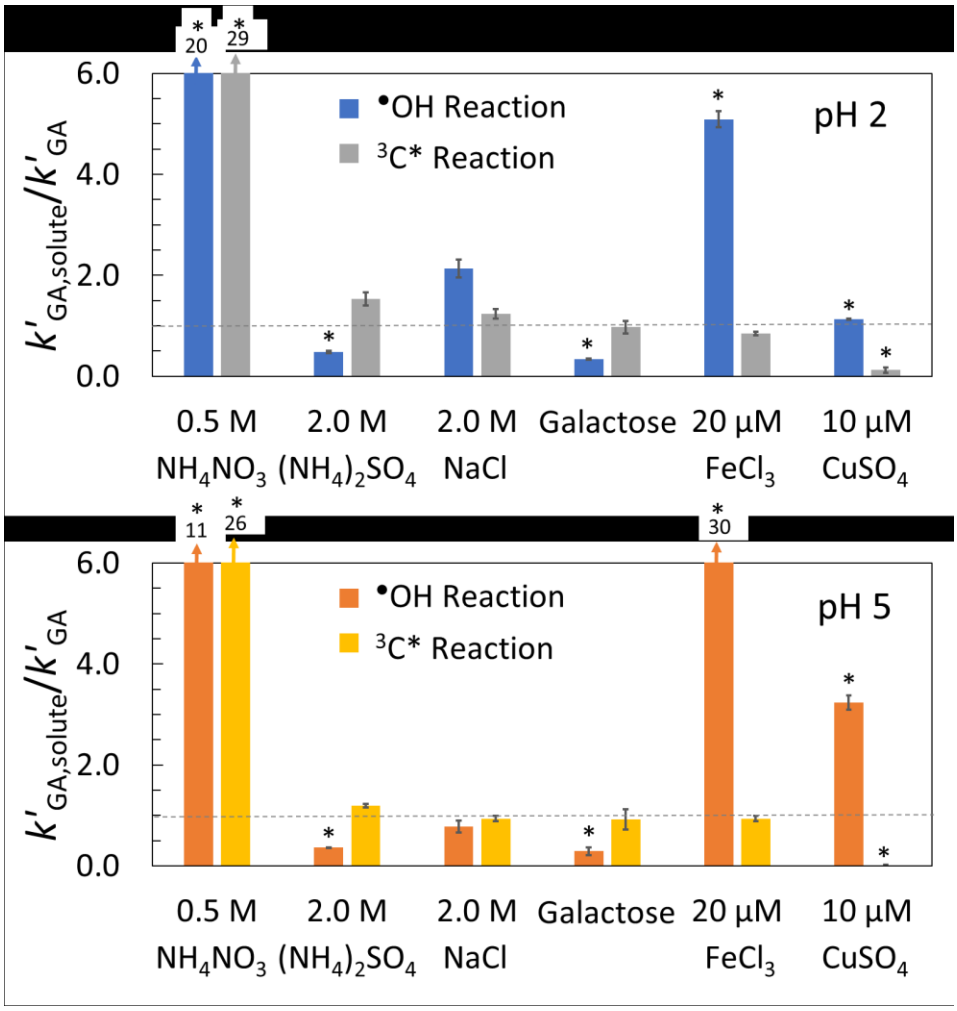

Figure S7: Comparison of the solute effects on the oxidation kinetics of guaiacylacetone (GA) by •OH and $^3C^*$. Solute experiments were measured at pH 2 (top panel) and pH 5 (bottom panel) for both oxidants. Galactose experiments were performed at two different concentrations: 1.0 mM galactose in the •OH experiments and 900 mM for $^3C^*$ experiments. For every solute, experiments were run in duplicate, with the average (± 1σ) shown in the figures. The dashed line at 1 represents the case where the solute did not affect GA loss. Bars with an asterisk are statistically different from 1 ($p < 0.05$).

Table S7: Measured •OH Concentrations in fog waters and PM. Data are shown in Figure S8 and Figure 5 in the main text.

Reference	Sample ID	P_{OH} [a] (10^{-10} M s^{-1})	P_{MT} [b] (10^{-10} M s^{-1})	k'_{OH} [c] (10^{5} s^{-1})	[OH] [d] (10^{-16} M)	Particle Mass/ Water Mass [e] (g-PM m^{-3}-air/ g-H_2O m^{-3}-air)	Sample Type and Location
Anastasio and McGregor 2001[11,f]	DA97-A01	9.7	13	15	15	6.4×10^{-5}	Fog waters from Davis, CA
	DA98-05F	12	21	19	18	1.4×10^{-4}	
	DA98-06F	11	24	19	18	1.6×10^{-4}	
	DA98-14F	3.3	14	6.8	26	7.7×10^{-5}	
Anastasio and Newberg 2007[12,g]	Stage 3					0.22	Extracts of marine PM from Bodega Bay, CA
	B9903	360	2000	4000	5.8		
	B9904	2600	2000	2600	17		
	Stage 2						
	B9903	170	310	1600	3.1		
	B9904	610	310	540	17		
	B9905	330	310	2600	2.4		
	Stage 2 + 3						
	B9801	280	220	350	14		
	B9802	940	220	2000	5.7		
	B9804	1600	220	3400	5.2		
	B9805	1000	220	2100	6.0		
	B9902	190	220	2700	1.5		
Arakaki et al. 2013[13,h]		4900	310	3500	15	0.52	Extracts of marine PM from Cape Hido, Japan
Kaur and Anastasio 2017[14,i]	UCD 1	3.9	9.6	8.6	16	4.2×10^{-5}	Fog waters from Davis, CA and Baton Rouge, LA
	UCD 2	2.3	19	6.0	35	1.1×10^{-4}	
	UCD 3	3.6	27	7.3	42	2.0×10^{-4}	
	UCD 4	4.4	23	13	21	1.6×10^{-4}	
	LSU1	6.9	1.1	6.2	28	4.8×10^{-5}	
	LSU2	1.3	6.3	5.0	15	2.2×10^{-5}	
	LSU3	1.3	14	3.5	43	7.3×10^{-5}	
	LSU4	3.6	12	6.7	23	5.9×10^{-5}	
Kaur et al. 2019[15,j]	PME1	1.0	9.6	6.3	17	4.2×10^{-5}	Extracts of winter PM from Davis, CA
	PME2	2.0	18	4.4	45	1.1×10^{-4}	
	PME3	15	38	19	28	3.3×10^{-4}	
	PME3D10	0.47	8.5	0.71	130	3.5×10^{-5}	
	PME3D2.5	3.1	20	9.4	25	1.3×10^{-4}	
	PME3D1.3	9.4	31	15	27	2.4×10^{-4}	
	PME3D0.5	27	70	38	25	8.4×10^{-4}	
	PME4	14	39	23	23	3.5×10^{-4}	
	PME5	4.6	21	16	16	1.3×10^{-4}	

	PME6	13	25	40	9.4	1.7×10^{-4}	

[a] P_{OH} is the rate of •OH photoproduction in samples. Values are the measured rates in the fog or PM extracts, except for the marine particles, where measured production rates in diluted extracts were adjusted to the expected airborne particle condition at 88% RH.

[b] Unless otherwise noted, P_{MT} is the rate of gas-to-drop partitioning of •OH determined using the Fuchs-Sutugin transition regime formula with an assumed gas-phase •OH concentration of 1×10^6 molecules cm^{-3} and a mass accommodation coefficient of 1.

[c] Pseudo-first-order rate constant for the destruction of •OH due to natural sinks. Values are the measured rate constants in the fog or PM extracts, except for the marine particles, where measured k'_{OH} values were adjusted to the expected airborne particle condition at 88% RH.

[d] Steady-state concentration of aqueous •OH, determined as P_{OH} / k'_{OH}.

[e] Particle mass-to-water mass ratio, determined as the ratio of the total dry particulate mass concentration (g-PM m^{-3}) divided by the liquid water content (LWC; g-H_2O m^{-3}).

[f] PM mass-to-water mass calculated by summing the PM species shown in Table 1 of the text with the LWC reported for each sample in Anastasio and McGregor. P_{OH} and k'_{OH} are summarized in Table 3.

[g] Sea-salt particle mass-to-water mass ratios calculated by using measurements from Table 4 in Newberg et al. (2005)[16] and estimating the LWC using Extended Aerosol Inorganics Model (E-AIM) Model IV (88% RH and 291.48 K). P_{OH} and k'_{OH} values are from Table 2 of Anastasio and Newberg (2007).[12] P_{MT} was estimated based on particle diameter using Figure 5 in the text.

[h] k'_{OH} reported here is an average value of Cape Hedo samples (n = 61). P_{OH} was reported in Arakaki et al. 2006.[17] P_{MT} was determined based on particle diameter using Figure 5 from Anastasio and Newberg, assuming a particle diameter range of 1.6 – 4.8 µm. We determined an average PM mass-to-water mass ratio by using E-AIM Model III (74% RH and 297 K; based on average ambient Cape Hedo measurements) to estimate the LWC for an aerosol containing the species reported in Table 1 of Arakaki et al. (2006).[17]

[i] P_{OH} and k'_{OH} for fog water samples are summarized in Table 2 from Kaur and Anastasio.[14] PM masses were determined by summing the mass of each species shown in Table 1. The LWC was estimated by calculating the sampling rate from data in Table 1 and correcting air samples with the sampling efficiency of the CASSC2.[14]

[j] The mass of extracted PM from each filter sample is summarized in Table S1 of Kaur et al. (2019).[15] P_{OH} and k'_{OH} for samples are summarized in Table S3. PME 1 to 6 samples were extracted with either 1 ml/filter (standard condition) or 2.5 mL/filter (dilute condition). A series of different extractions were performed on PME sample 3, with volumes between 0.5 and 10 mL; these are labeled PME3D*x*, with *x* being the volume used for extraction.[15]

Table S8: Modeled aqueous •OH concentrations in clouds, fog, and PM. These data are presented graphically in Figure S8 and Figure 5 in the main text.

Study	[•OH] (10^{-14} M)	Particle Mass/Water Mass [a] (g-Particle mass m^{-3}-air/ g-water mass m^{-3}-air)	Sample Type
Jacob et al. 1989[18,b]	1.6	2.7×10^{-4}	continental fog
Seinfeld and Pandis 1989[19,c]	5.6	5.8×10^{-6}	remote cloud
Warneck 1999[20,d]	5.0 2.6	2.8×10^{-4} 2.8×10^{-4}	remote – no metals remote – with metals
Monod and Carlier 1999[21,e]	1.6	2.7×10^{-4}	fog
Herrmann et al. 2000[22,f]	200 170 140	1.4×10^{-4} 7.1×10^{-5} 7.2×10^{-5}	marine cloud remote cloud urban cloud
Warneck 2003[23,g]	18	2.8×10^{-4}	marine cloud
Warneck 2005[24,h]	39 0.04	2.0×10^{-5} 0.2	marine cloud marine particle
Herrmann et al. 2005[25,i]	11 1.1 73	7.1×10^{-5} 8.4×10^{-5} 1.4×10^{-4}	remote cloud continental cloud marine cloud
Ervens and Volkamer 2010[26,j]	10 600	2.8×10^{-5} 2.75	cloud PM
Ervens et al. 2014[27,k]	140 320	9.0×10^{-7} 0.50	cloud PM
Barth et al. 2021[28,l]	25(CAPRAM) 500(CLEPS) 300(GAMMA) 40(Barth) 10(Ervens)	2.8×10^{-6}	remote cloud

[a] Particle mass-to-water mass ratio, calculated as the total dry particulate mass concentration (g-PM m^{-3}) divided by the liquid water content (LWC; g-H_2O m^{-3}).
[b] Noontime [•OH] value. PM mass-to-water mass ratio estimated using Table 2.
[c] [•OH] estimated from reported CH_3OH decay. PM mass-to-water mass ratio estimated using Table 1 and the LWC reported in the text.
[d] Midday [•OH] value. PM mass estimated using Table 6 and LWC reported in the text.
[e] PM mass-to-water mass ratio calculated using Table 7 in the text as well as Henry's law constants to estimate aqueous concentrations of gaseous organics. LWC was directly reported.
[f] PM mass estimated using Table 1.
[g] PM mass-to-water mass ratio estimated using Table 6 and the same LWC from Warneck 1999.[20]

[h] [•OH] reported for noontime value. PM mass estimated using Table 1 in the text. LWC is reported for both conditions.

[i] PM mass estimated from the initial concentration of aqueous species in CAPRAM 2.3 for a given scenario. The LWC is reported in the paper.

[j] We used the PM mass concentration reported in the text for both the cloud and PM conditions.

[k] PM mass estimated using Figure 7 in the text.

[l] PM mass calculated using the species shown in Table S4 from the Supporting Information S3.

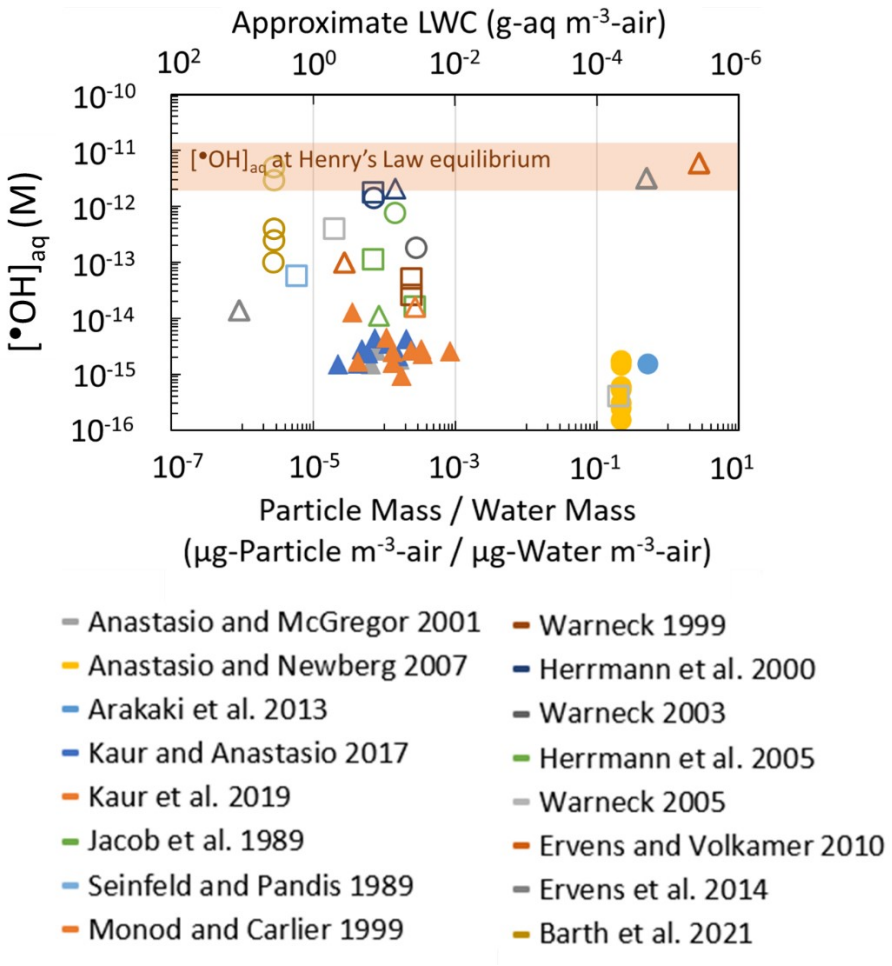

Figure S8: $^{\bullet}$OH concentrations from measured (filled markers) and modeling studies (open markers) as a function of dry particle mass/liquid water mass ratio. The top axis indicates approximate liquid water content (LWC; g-aq m^{-3}-air), calculated for an assumed PM mass concentration of 10 µg-PM m^{-3}. Sample types include urban samples (triangles), marine samples (squares), and remote continental samples (circles). The orange box represents the $^{\bullet}$OH concentration calculated assuming Henry's Law equilibrium with gas-phase $^{\bullet}$OH concentrations from the modeling studies, (1.3 – 7.4) x 10^6 molecules cm^{-3},[18,19,23,24,26,27] and a Henry's law constant of 38.5 M atm^{-1}.[29]

References

(1) Ma, L.; Guzman, C.; Niedek, C.; Tran, T.; Zhang, Q.; Anastasio, C. Kinetics and Mass Yields of Aqueous Secondary Organic Aerosol from Highly Substituted Phenols Reacting with a Triplet Excited State. *Environ. Sci. Technol.* **2021**, *55*, 5772-5781.

(2) Smith, J. D.; Kinney, H.; Anastasio, C. Aqueous benzene-diols react with an organic triplet excited state and hydroxyl radical to form secondary organic aerosol. *Phys. Chem. Chem. Phys.* **2015**, *17*, 10227–10237.

(3) Herrmann, H.; Hoffmann, D.; Schaefer, T.; Bräuer, P.; Tilgner, A. Tropospheric aqueous-phase free-radical chemistry: radical sources, spectra, reaction kinetics and prediction tools. *ChemPhysChem* **2010**, *11*, 3796–3822.

(4) Ross, F.; Ross, A. B. *Selected specific rates of reactions of transients from water in aqueous solution. III. Hydroxyl radical and perhydroxyl radical and their radical ions*; Historical Energy Database (United States), 1977.

(5) Field, R. J.; Raghavan, N. V.; Brummer, J. G. A pulse radiolysis investigation of the reactions of bromine dioxide radical (BrO2.cntdot.) with hexacyanoferrate(II), manganese(II), phenoxide ion, and phenol. *J. Phys. Chem.* **1982**, *86*, 2443–2449.

(6) Land, E. J.; Ebert, M. Pulse radiolysis studies of aqueous phenol. Water elimination from dihydroxycyclohexadienyl radicals to form phenoxyl. *Trans. Faraday Soc.* **1967**, *63*, 1181.

(7) Wander, R.; Neta, P.; Dorfman, L. M. Pulse radiolysis studies. XII. Kinetics and spectra of the cyclohexadienyl radicals in aqueous benzoic acid solution. *J. Phys. Chem.* **1968**, *72*, 2946–2949.

(8) Yu, L.; Smith, J.; Laskin, A.; George, K. M.; Anastasio, C.; Laskin, J.; Dillner, A. M.; Zhang, Q. Molecular transformations of phenolic SOA during photochemical aging in the aqueous phase: competition among oligomerization, functionalization, and fragmentation. *Atmos. Chem. Phys.* **2016**, *16*, 4511–4527.

(9) Smith, J. D.; Sio, V.; Yu, L.; Zhang, Q.; Anastasio, C. Secondary organic aerosol production from aqueous reactions of atmospheric phenols with an organic triplet excited state. *Environ. Sci. Technol.* **2014**, *48*, 1049–1057.

(10) Smith, J. D.; Kinney, H.; Anastasio, C. Phenolic carbonyls undergo rapid aqueous photodegradation to form low-volatility, light-absorbing products. *Atmos. Environ.* **2016**, *126*, 36–44.

(11) Anastasio, C.; McGregor, K. G. Chemistry of fog waters in California's Central Valley: 1. In situ photoformation of hydroxyl radical and singlet molecular oxygen. *Atmos. Environ.* **2001**, *35*, 1079–1089.

(12) Anastasio, C.; Newberg, J. T. Sources and sinks of hydroxyl radical in sea-salt particles. *J. Geophys. Res. Atmos.* **2007**, *112*.

(13) Arakaki, T.; Anastasio, C.; Kuroki, Y.; Nakajima, H.; Okada, K.; Kotani, Y.; Handa, D.; Azechi, S.; Kimura, T.; Tsuhako, A.; et al. A general scavenging rate constant for reaction of hydroxyl radical with organic carbon in atmospheric waters. *Environ. Sci. Technol.* **2013**, *47*, 8196–8203.

(14) Kaur, R.; Anastasio, C. Light absorption and the photoformation of hydroxyl radical and singlet oxygen in fog waters. *Atmos. Environ.* **2017**, *164*, 387–397.

(15) Kaur, R.; Labins, J. R.; Helbock, S. S.; Jiang, W.; Bein, K. J.; Zhang, Q.; Anastasio, C. Photooxidants from brown carbon and other chromophores in illuminated particle extracts. *Atmos. Chem. Phys.* **2019**, *19*, 6579–6594.

(16) Newberg, J. T.; Matthew, B. M.; Anastasio, C. Chloride and bromide depletions in sea-salt particles over the northeastern Pacific Ocean. *J. Geophys. Res. Atmos.* **2005**, *110*.

(17) Arakaki, T.; Kuroki, Y.; Okada, K.; Nakama, Y.; Ikota, H.; Kinjo, M.; Higuchi, T.; Uehara, M.; Tanahara, A. Chemical composition and photochemical formation of hydroxyl radicals in aqueous extracts of aerosol particles collected in Okinawa, Japan. *Atmos. Environ.* **2006**, *40*, 4764–4774.

(18) Jacob, D. J.; Gottlieb, E. W.; Prather, M. J. Chemistry of a polluted cloudy boundary layer. *J. Geophys. Res. Atmos.* **1989**, *94*, 12975–13002.

(19) Pandis, S. N.; Seinfeld, J. H. Sensitivity analysis of a chemical mechanism for aqueous-phase atmospheric chemistry. *J. Geophys. Res. Atmos.* **1989**, *94*, 1105–1126.

(20) Warneck, P. The relative importance of various pathways for the oxidation of sulfur dioxide and nitrogen dioxide in sunlit continental fair weather clouds. *Phys. Chem. Chem. Phys.* **1999**, *1*, 5471–5483.

(21) Monod, A.; Carlier, P. Impact of clouds on the tropospheric ozone budget: Direct effect of multiphase photochemistry of soluble organic compounds. *Atmos. Environ.* **1999**, *33*, 4431–4446.

(22) Herrmann, H.; Ervens, B.; Jacobi, H.-W.; Wolke, R.; Nowacki, P.; Zellner, R. CAPRAM2.3: A chemical aqueous phase radical mechanism for tropospheric chemistry. *Journal of Atmospheric Chemistry* **2000**, *36*, 231–284.

(23) Warneck, P. In-cloud chemistry opens pathway to the formation of oxalic acid in the marine atmosphere. *Atmos. Environ.* **2003**, *37*, 2423–2427.

(24) Warneck, P. Multi-Phase Chemistry of C2 and C3 Organic Compounds in the Marine Atmosphere. *J. Atmos. Chem.* **2005**, *51*, 119–159.

(25) Herrmann, H.; Tilgner, A.; Barzaghi, P.; Majdik, Z.; Gligorovski, S.; Poulain, L.; Monod, A. Towards a more detailed description of tropospheric aqueous phase organic chemistry: CAPRAM 3.0. *Atmos. Environ.* **2005**, *39*, 4351–4363.

(26) Ervens, B.; Volkamer, R. Glyoxal processing by aerosol multiphase chemistry: towards a kinetic modeling framework of secondary organic aerosol formation in aqueous particles. *Atmos. Chem. Phys.* **2010**, *10*, 8219–8244.

(27) Ervens, B.; Sorooshian, A.; Lim, Y. B.; Turpin, B. J. Key parameters controlling OH-initiated formation of secondary organic aerosol in the aqueous phase (aqSOA). *J. Geophys. Res. Atmos.* **2014**, *119*, 3997–4016.

(28) Barth, M. C.; Ervens, B.; Herrmann, H.; Tilgner, A.; McNeill, V. F.; Tsui, W. G.; Deguillaume, L.; Chaumerliac, N.; Carlton, A.; Lance, S. M. Box model intercomparison of cloud chemistry. *J. Geophys. Res* **2021**, *126*.

(29) Sander, R. Compilation of Henry's law constants (version 4.0) for water as solvent. *Atmos. Chem. Phys.* **2015**, *15*, 4399–4981.